Precision measurement of forward Z boson production in proton-proton collisions at $\sqrt{s} = 13$ TeV

The LHCb collaboration

E-mail: hang.yin@cern.ch

ABSTRACT: A precision measurement of the Z boson production cross-section at $\sqrt{s} = 13$ TeV in the forward region is presented, using pp collision data collected by the LHCb detector, corresponding to an integrated luminosity of $5.1\,\text{fb}^{-1}$. The production cross-section is measured using $Z \to \mu^+\mu^-$ events within the fiducial region defined as pseudorapidity $2.0 < \eta < 4.5$ and transverse momentum $p_\text{T} > 20\,\text{GeV}/c$ for both muons and dimuon invariant mass $60 < M_{\mu\mu} < 120\,\text{GeV}/c^2$. The integrated cross-section is determined to be

$$\sigma(Z \to \mu^+\mu^-) = 196.4 \pm 0.2 \pm 1.6 \pm 3.9\,\text{pb},$$

where the first uncertainty is statistical, the second is systematic, and the third is due to the luminosity determination. The measured results are in agreement with theoretical predictions within uncertainties.

Contents

1   Introduction

Precision measurements of the single Z boson[1] production cross-section at the CERN Large Hadron Collider (LHC) provide an important test of the quantum chromodynamics (QCD) and electroweak (EW) sectors of the Standard Model. Theoretical predictions for the Z boson production cross-section are available up to next-to-next-to-next-to-leading order in perturbative QCD [1, 2] and have comparable precision as the measured results to date. Further validations and tests on theoretical predictions [3–9] require precision measurements of the Z boson production cross-section in different experiments. The LHCb collaboration has previously reported the measurement of the W boson mass [10], using a data sample corresponding to an integrated luminosity of $1.7\,\mathrm{fb}^{-1}$, and sizable uncertainties from parton distribution functions (PDFs) and boson p_{T} modelling are seen. A measurement of the Z boson production cross-section will provide information to reduce these uncertainties, and the future measurements of the W boson mass and weak mixing angle [11] at LHCb could also benefit from this measurement.

The Z boson candidates collected with the LHCb detector are highly boosted, and produced by a parton with large Bjorken-x and another with small x. The Bjorken-x is the fraction of the proton momentum carried by a parton. Therefore, a precision measurement of Z boson production cross-section with the LHCb detector is particularly sensitive to PDFs, especially in the very large and small x ranges. The PDFs are constrained by the results from deep inelastic scattering and hadron collider experiments [12–27]. However, these measurements provide limited information for the PDFs for very large x (up to ~ 0.8) or very small x ($\sim 5 \times 10^{-5}$), which leads to large PDF uncertainty, and consequently a large uncertainty in theoretical predictions of vector boson production cross-section in the forward region. As the LHCb detector has fully instrumented coverage in the forward region, with complementary acceptance compared to the ATLAS and CMS detectors, the collected Z boson candidates can provide unique and important information for the determining the PDFs. Previous measurements of single W and Z production by the LHCb collaboration [28–33] have been included in PDF calculations [34–37], and contribute significantly to the determination of the valence quark PDFs at large and small values of x. Furthermore, the LHCb measurements constrain strange and charm PDFs at high x, including intrinsic charm [38, 39]. Recently, the SeaQuest collaboration [40] reported a measurement of the Drell-Yan process, which is sensitive to $\bar{d}/\bar{u}$ PDF ratio. Tensions between the SeaQuest [40] and NuSea [41] results in the large x region are observed. Since both results have large contributions from nuclear effects, LHCb measurements using the proton-proton (pp) collision data can provide complementary constraints in that x region.

In this article, the integrated and differential Z boson production cross-sections are measured at the Born level in QED using pp collision data collected by the LHCb detector at a centre-of-mass energy $\sqrt{s} = 13\,\mathrm{TeV}$ in 2016, 2017 and 2018, corresponding to an integrated luminosity of $5.1 \pm 0.1\,\mathrm{fb}^{-1}$ [42]. The production cross-section is measured in a fiducial region that closely matches the acceptance of the LHCb detector. The fiducial region is defined as pseudorapidity $2.0 < \eta < 4.5$ and transverse momentum $p_{\mathrm{T}} > 20\,\mathrm{GeV}/c$ for

---

[1]In this article, the label Z boson is defined to include contributions from virtual photons and interference between them.

both muons and dimuon invariant mass $60 < M_{\mu\mu} < 120\,\mathrm{GeV}/c^2$. A similar measurement using the LHCb dielectron events is foreseen in future. The differential cross-section is measured as a function of the Z boson rapidity (y^Z), transverse momentum (p_T^Z) and ϕ_η^*. The observable ϕ_η^*, which was first measured by the D0 [43] experiment, probes similar physics as the Z boson p_T, but is an angular variable that can be measured with better resolution by collider detectors. It is defined as

$$\phi_\eta^* = \tan((\pi - \Delta\phi^{\ell\ell})/2)\sin(\theta_\eta^*), \tag{1.1}$$

where $\Delta\phi^{\ell\ell}$ is the difference in azimuthal angle, ϕ, between the two muons, θ_η^* is the scattering angle of the muons with respect to the proton beam direction in the rest frame of the dimuon system. The variable θ_η^* is defined by $\cos(\theta_\eta^*) = \tanh[(\eta^- - \eta^+)/2]$, where η^- and η^+ are the pseudorapidities of the negatively and positively charged muon, respectively. Moreover, double differential cross-sections of Z boson production in regions of y^Z and p_T^Z, and of y^Z and ϕ_η^*, are measured for the first time in the LHCb forward acceptance.

2 Detector and simulation

The LHCb detector [44, 45] is a single-arm forward spectrometer covering the pseudorapidity range $2 < \eta < 5$, designed for the study of particles containing b or c quarks. The detector includes a high-precision tracking system consisting of a silicon-strip vertex detector surrounding the pp interaction region [46], a large-area silicon-strip detector (TT) [47], located upstream of a dipole magnet with a bending power of about $4\,\mathrm{Tm}$, and three stations of silicon-strip detectors and straw drift tubes [48] placed downstream of the magnet. The tracking system provides a measurement of the momentum, p, of charged particles with a relative uncertainty that varies from 0.5% at low momentum to 1.0% at $200\,\mathrm{GeV}/c$. The minimum distance of a track to a primary pp collision vertex (PV), the impact parameter (IP), is measured with a resolution of $(15 + 29/p_T)\,\mu\mathrm{m}$, where p_T is the component of the momentum transverse to the beam, in GeV/c. Photons, electrons and hadrons are identified by a calorimeter system consisting of scintillating-pad and preshower detectors, an electromagnetic and a hadronic calorimeter. Muons are identified by a system composed of alternating layers of iron and multiwire proportional chambers [49]. The online event selection is performed by a trigger [50], which consists of a hardware stage, based on information from the calorimeter and muon systems, followed by a software stage, which applies a full event reconstruction.

Simulation is required to model the effects of the detector acceptance and the imposed selection requirements. In the simulation, pp collisions are generated using PYTHIA [51] with a specific LHCb configuration [52]. The final state radiation is generated using PHOTOS [53]. The interaction of the generated particles with the detector, and its response, are implemented using the GEANT4 toolkit [54] as described in ref. [55].

3 Reconstruction and selection

The online event selection is performed by the muon triggers. At the hardware trigger stage, candidates are required to have a muon object with high p_T. The muon candidate
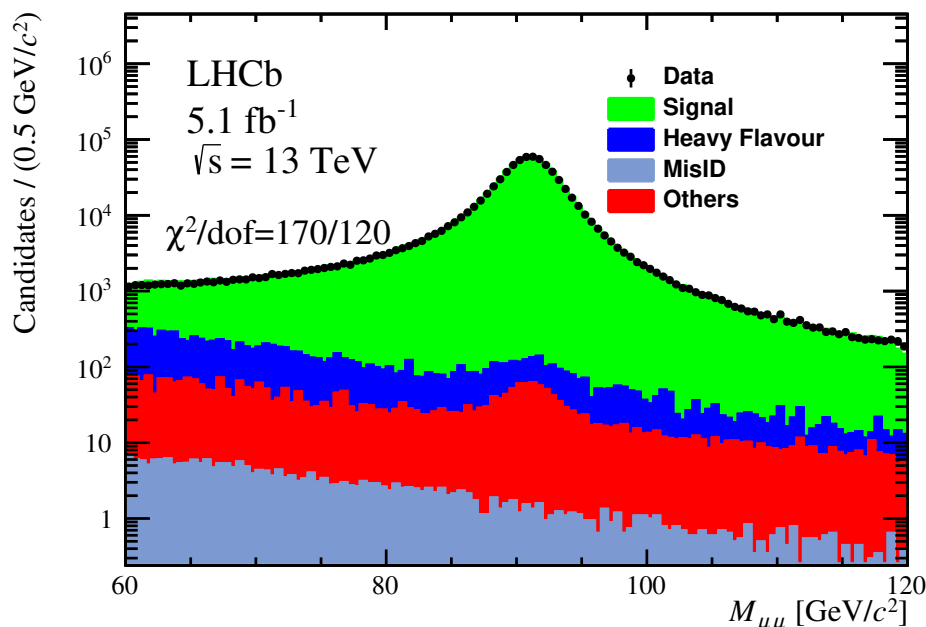
Figure 1. Comparison of the invariant mass distribution between data and the sum of signal and background contributions for the selected $Z \to \mu^+\mu^-$ candidates.

must satisfy $p_T > 6 \, \text{GeV}/c$, $p > 8 \, \text{GeV}/c$, with a good track fit quality in the first software trigger stage. While in the second software trigger stage, the muon candidate is further required to satisfy $p_T > 12.5 \, \text{GeV}/c$. For a $Z \to \mu^+\mu^-$ candidate, at least one of the muons is required to pass both hardware and software trigger decision stages.

To select a $Z \to \mu^+\mu^-$ sample with high purity, candidates are required to have a pair of well-reconstructed tracks of opposite charge identified as muons. The invariant mass of two muons must be in the range $60 < M_{\mu\mu} < 120 \, \text{GeV}/c^2$. Muon tracks must have a transverse momentum $p_T > 20 \, \text{GeV}/c$ and pseudorapidity in the range $2.0 < \eta < 4.5$. The relative uncertainty in the momentum measurement for each muon is required to be less than 10%. In total, 796 thousand $Z \to \mu^+\mu^-$ candidates are selected, and the dimuon invariant mass distribution of the selected candidates is shown in figure 1.

4 Background

4.1 Heavy flavour background

Heavy flavour production ($b\bar{b}$ and $c\bar{c}$ quark pairs) has a large branching fraction into semileptonic decays, and is one of the largest background sources to the $Z \to \mu^+\mu^-$ process. This contribution is estimated from data, using two control samples enriched in heavy flavour.

The event selection requirements described in section 3 are used to select two control samples, in which the dimuon invariant mass requirement is changed to $50 < M_{\mu\mu} < 80 \, \text{GeV}/c^2$. The first control sample is selected by requiring that the data candidate must have a primary vertex with a low fit quality. For signal events, the two muons originate at the

primary vertex, while muons arising from decays of heavy hadrons do not, and thus have a low vertex fit quality. The second sample is selected by requiring that the two muons are not spatially isolated ($I_\mu < 0.7$) from other activity in the event. The muon isolation variable, I_μ, is defined as the ratio of the muon p_T to the p_T of the vector sum of all charged particles p_T in a cone of size 0.5 in the $\eta - \phi$ coordinates around the muon, where ϕ is the azimuthal angle of the muon.

The event yields of these two control samples are determined by fitting the dimuon invariant mass distribution with an exponential function, followed by an extrapolation of the fitted results to the signal region ($60 < M_{\mu\mu} < 120$ GeV/c^2). These event yields are corrected with the corresponding efficiency of the vertex and muon isolation selections, where the efficiency of the muon isolation (vertex) selection is calculated by applying the muon isolation requirement (vertex fit quality requirement) to the first (second) control sample.

Studies on these two sub-samples are consistent, and the averaged value of the estimated background yields is taken as background contribution from the heavy flavour process, which is determined to be $(1.0 \pm 0.1)\%$ for the selected $Z \to \mu^+\mu^-$ sample.

4.2 Background from misidentified hadrons

Charged pions or kaons could be misidentified as muons and contribute to the selected $Z \to \mu^+\mu^-$ sample if they decay in flight before reaching the muon stations or if they have sufficient energy to traverse the calorimeters and be detected in the muon stations. The contribution from the combinatorial background including misidentified hadrons and $B - \bar{B}$ mixing is determined using pairs of same-sign muons in the data. It is assumed that the charges of the selected muons are uncorrelated for these sources, which is validated by comparing the numbers of $\mu^+\mu^+$ and $\mu^-\mu^-$ candidates. The difference between the number of $\mu^+\mu^+$ and $\mu^-\mu^-$ candidates is assigned as an additional uncertainty in the background contribution.

However, sizable contributions from heavy flavour processes (i.e., a muon from heavy flavour decay combined with a misidentified hadron) in the same-sign events are expected. To remove the double counting of the heavy flavour background in the background study, a method similar to the one described in section 4.1 is used, by inverting the vertex fit quality and the muon isolation requirements to obtain two background samples enhanced in same-sign events. The contribution from the heavy flavour processes in the same-sign events is determined to be $(95 \pm 4)\%$.

After removing the contribution from heavy flavour processes, the contribution from misidentified hadrons is determined to be 0.04% with negligibly small uncertainty.

4.3 Background from other physics processes

Background contributions from $t\bar{t}$, W^+W^-, $W^\pm Z$, ZZ, and $Z \to \tau^+\tau^-$ processes are estimated using simulation. The number of background events from the $Z \to \tau^+\tau^-$ process, which subsequently decay to dimuons that pass the event selection, is determined using simulation, taking into account of the integrated luminosity and the predicted Z boson production cross-section at next-to-next-to-leading-order (NNLO) [56]. The contribution

from $t\bar{t}$ production, where both top quarks produce $W^{\pm}$ bosons and then decay to muons, is estimated using simulation and the $t\bar{t}$ production cross-section measured by the LHCb collaboration [57]. The background contribution from diboson (W^+W^-, $W^{\pm}Z$, and ZZ) decays is estimated using a similar method.

Summing contributions from the heavy flavour, misidentified hadrons and physics processes, the total background contribution to the $Z \to \mu^+\mu^-$ sample in the mass range 60–120 GeV/c^2 is determined to be $(1.5 \pm 0.1)\%$.

5 Methods

The differential cross-section is defined in interval regions of observable a (y^Z, p_T^Z or ϕ_η^*) as

$$\frac{d\sigma_{Z\to\mu^+\mu^-}}{da} = \frac{N_Z \cdot f_{\text{FSR}}^Z}{\mathcal{L} \cdot \varepsilon^Z \cdot \Delta a}, \tag{5.1}$$

where N_Z is the signal yield in a given region, f_{FSR}^Z is the final state radiation (FSR) correction factor (as discussed in section 5.4), $\mathcal{L}$ is the integrated luminosity, Δa is the interval width of the observable in a given region (as presented in tables 2 through 6 in appendix A), and ε^Z is the total efficiency in this region. The integrated cross-section is obtained by summing over all regions.

The differential production cross-section is measured in 18 regions of y^Z, from 2.0 to 4.5 with region width of 0.125, and of 0.25 above 4.0. The differential production cross-section as a function of p_T^Z is measured in 14 regions [0.0, 2.2, 3.4, 4.6, 5.8, 7.2, 8.7, 10.5, 12.8, 15.4, 19.0, 24.5, 34.0, 63.0, 270.0] GeV/c. The differential production cross-section as a function of ϕ_η^* is measured in 15 regions [0.002, 0.01, 0.02, 0.03, 0.05, 0.07, 0.10, 0.15, 0.20, 0.30, 0.40, 0.60, 0.80, 1.20, 2.00, 4.00]. These region schemes are chosen based on the detector resolution and sample size of each region. The double-differential cross-section measurements are performed in five y^Z regions of width 0.5. In each y^Z region, the above 14 regions of p_T^Z and 15 regions of ϕ_η^* are used.

5.1 Detector alignment and momentum scale calibration

Starting with taking data in 2015, the LHCb collaboration employs a novel online alignment procedure [58], which is used to obtain a stable performance of the detector. However, as the core physics programme is heavy flavour physics, the detector calibrations are not optimized for EW physics. In particular, the momentum scale calibration for the high-momentum muons that form the main signature of the $W^{\pm}$ and Z boson decays, can be improved significantly with an additional detector alignment.

To correct the detector misalignment effects, the mass peak position of the selected $Z \to \mu^+\mu^-$ candidates is calibrated in different kinematic and geometric regions to the world averaged value [59]. The impact on the integrated cross-section measurement from this correction is found to be negligible. However, with finer region schemes, in all of the differential cross-section measurements, this uncertainty has to be considered as one of the systematic uncertainties.

5.2 Efficiency

Several corrections are developed and applied to the simulation, to achieve a better modelling of the LHCb detector response. The event selection efficiencies are determined for the muon trigger, as well as the tracking and identification requirements, using the $Z \to \mu^+\mu^-$ data candidates with the tag-and-probe method [60].

In the determination of the tracking efficiency, a particle reconstructed in all tracking subdetectors, having passed the muon trigger and muon identification requirements, is used as the tag. An object reconstructed by combining hits in the muon stations and the TT station, denoted as MuonTT track, acts as the probe. The probe is then tested for the presence of an associated track, by searching for all reconstructed tracks linked to muon segments which have more than 40% of their hits in the muon stations and 60% of their hits in the TT station in common with the MuonTT track. As described in ref. [60], the tracking efficiency is calculated as the fraction of probe candidates matched with a reconstructed track.

This tag-and-probe tracking efficiency is further corrected to remove bias from the method itself. The correction is the ratio of the tracking efficiency estimated using truth level information to that of the tag-and-probe method, where the truth level tracking efficiency is defined as the fraction of simulated muon with sufficient hits in the muon and TT stations to satisfy the requirements of the track matching. There are two effects: a bias and a track matching correction. The bias correction takes into account the fact that the tracking efficiency is estimated using the MuonTT track, but not all of the muon tracks have an associated MuonTT track. The track matching correction takes into account the inefficiency from the matching conditions. The determined muon tracking efficiency varies from 94% to 97% in different kinematic regions.

To determine the muon trigger and identification efficiency, the tag particle is selected from a particle reconstructed in all tracking subdetectors, by requiring it to be identified and triggered as muon, while the probe particle must be a track with good quality. The track must be identified as a muon when studying trigger efficiency. Both the tag and probe particles are further required to have $p_{\rm T}$ greater than $20\,{\rm GeV}/c$, η in a range from 2.0 to 4.5, and a relative momentum uncertainty less than 10%. The invariant mass of the tag and probe candidates is required to be in the range from 60 to $120\,{\rm GeV}/c^2$. To suppress background further, the tag and probe are required to have an azimuthal separation, $|\Delta\phi|$, greater than 2.7 radians. The efficiency is calculated as the ratio of the number of probes within the selected sample satisfying the muon trigger and identification requirements to the number of probes. The determined trigger and identification efficiency per-muon varies from 60% to 85%, and 65% to 96% in different kinematic regions, respectively.

The total efficiency ε^Z depends on the pseudorapidities of the two final-state muons and can be written as:

$$\varepsilon^Z = \left(\varepsilon^{\mu^+}_{\rm track} \cdot \varepsilon^{\mu^-}_{\rm track}\right) \cdot \left(\varepsilon^{\mu^+}_{\rm ID} \cdot \varepsilon^{\mu^-}_{\rm ID}\right) \cdot \left(\varepsilon^{\mu^+}_{\rm trig} + \varepsilon^{\mu^-}_{\rm trig} - \varepsilon^{\mu^+}_{\rm trig} \cdot \varepsilon^{\mu^-}_{\rm trig}\right), \tag{5.2}$$

where $\varepsilon^{\mu^\pm}_{\rm track}$, $\varepsilon^{\mu^\pm}_{\rm ID}$, and $\varepsilon^{\mu^\pm}_{\rm trig}$ are the calculated efficiencies of muon track reconstruction, muon identification, and muon trigger, respectively.
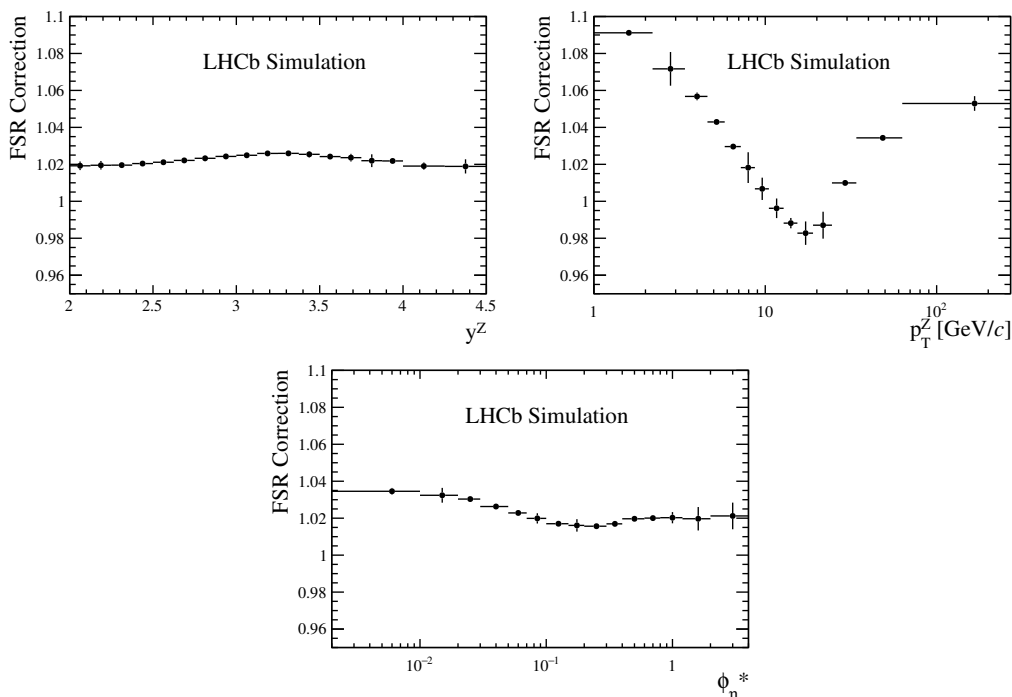
Figure 2. Final state radiation correction estimated for the (top-left) y^Z, (top-right) p_T^Z, and (bottom) ϕ_η^* differential cross-section measurements. The error bars represent the total (statistical and systematic) uncertainties.

5.3 Unfolding

The detector resolution effects could introduce a interval-to-interval migration between regions. This effect is corrected with the Bayesian unfolding method [61]. Because of the good angular resolution of the LHCb detector, negligible migration effects are observed in y^Z and ϕ_η^* measurements. Therefore, unfolding correction is applied only to the differential cross-section measured as a function of p_T^Z.

5.4 Final state radiation correction

The measured cross-section is corrected to the Born level in QED, so that it can be directly compared with different theoretical predictions. The final-state radiation correction is developed and applied to the measurements, by comparing the RESBOS [62] predictions with and without the implementation of PHOTOS [53], which corrects the bare level muon to the Born level. The FSR corrections in regions of y^Z, p_T^Z, and ϕ_η^* are shown in figure 2. The corrections for single- and double-differential cross-section measurements are presented in appendix A.

6 Systematic uncertainty

Various sources of systematic uncertainty in the cross-section measurement are estimated and combined in quadrature. These include uncertainty from background estimation, de-

tector alignment and momentum scale calibration, efficiency, unfolding, closure test, the FSR correction and luminosity.

6.1 Background

In the heavy flavour background determination, the averaged yield is used as the background contribution. Its uncertainty is taken as the difference of the background yields estimated using the two control samples. Furthermore, the mass region and the selection requirements of the control samples are varied and the difference is taken as an additional systematic uncertainty.

For the hadron misidentification and other background estimated from simulation, a systematic uncertainty is assigned to take into account the limited sample size of the same-sign data and simulation. Furthermore, the difference between the number of $\mu^+\mu^+$ and $\mu^-\mu^-$ events is taken as an additional uncertainty. For background estimated from the simulation, uncertainty from the theoretical predictions are also taken into account.

6.2 Detector alignment and momentum scale calibration

To estimate a systematic uncertainty for the detector alignment, the data sample is divided into two independent sub-samples. Then, a new alignment correction is developed using one of these sub-samples. The new determined correction is applied to the other sub-sample, and *vice versa*. The difference in the measurements using these two alignment corrections are taken as systematic uncertainty. The uncertainty from alignment and calibration is found to be negligible in the integrated cross-section measurement, and is determined for the differential cross-section measurements.

6.3 Efficiency correction

The efficiencies of track reconstruction, identification and trigger of the high p_T muons are directly measured from data using the $Z \to \mu^+\mu^-$ events. A systematic uncertainty is assigned for variations due to the limited size of the control samples, which is determined to be 0.05% for trigger efficiency, 0.11% for identification efficiency, and 0.29% for tracking efficiency.

The measured data efficiency is corrected for bias from the method itself. The correction developed from the simulation sample is broken down into the bias correction and the track matching correction. These two corrections are estimated using the simulation sample, and applied to the measured tag-and-probe efficiency. Differences between the simulation truth level efficiency and the corrected tag-and-probe efficiency of the simulation sample are assigned as systematic uncertainty. Furthermore, differences between the matching efficiency and the MuonTT track finding efficiency estimated from data and simulation samples are also considered as uncertainty. Finally, the estimated systematic uncertainty in tracking efficiency for each muon is determined to be 0.47%, which is one of dominant source of systematic uncertainty.

In total, the uncertainty from the efficiency corrections is determined to be 0.77% in the integrated cross-section measurement.

Source	$\Delta\sigma/\sigma$ [%]
Statistical	0.11
Background	0.06
Alignment & calibration	—
Efficiency	0.77
Closure	0.23
FSR	0.15
Total Systematic (excl. lumi.)	0.82
Luminosity	2.00
Total	2.16

Table 1. Relative uncertainty for the integrated $Z \to \mu^+\mu^-$ cross-section measurement. The total uncertainty is the quadratic sum of uncertainties from statistical, systematic and luminosity contributions.

6.4 Closure test

As one-dimensional efficiency corrections in muon η regions are used, possible additional dependence of efficiencies is not accounted for. To check effects from the multi-dimensional efficiency dependence, i.e. muon η and p_T regions, the number of reconstructed events in simulation is corrected using the efficiencies determined from the simulation, and compared to the yield at generator level. The differences, which show no evidence of a systematic trend across the regions, are assigned as uncertainty.

6.5 Other sources of systematic uncertainty

To estimate the uncertainty from unfolding, the p_T distribution is unfolded using the bin-by-bin correction approach [63]. The difference of results with respect to the Bayesian approach is taken as a systematic uncertainty on the differential cross-section measured in p_T^Z region.

The systematic uncertainty from the FSR correction is estimated by comparing the default correction with that calculated using the Powheg generator, with the Pythia showering. The differences of FSR corrections between ResBos with Photos and Powheg with Pythia are taken as systematic uncertainty.

For the data sample used, the luminosity is determined with a precision of 2.0% [42]. The statistical and systematic uncertainties in the integrated cross-section measurement are presented in table 1.

7 Results

The datasets that were collected in 2016, 2017 and 2018 are considered as independent datasets, which are used to perform cross-section measurements and combined to get results of the full dataset. In the combination of integrated cross-section measurements obtained from the different datasets, the systematic uncertainties from FSR, background modelling, luminosity, and closure test, are treated as 100% correlated between different datasets,

and other systematic uncertainties are assumed to be uncorrelated. The combination is performed using the Best Linear Unbiased Estimator (BLUE) method [64, 65].

7.1 Differential cross-section results

The measured differential cross-section in regions of y^Z is shown in figure 3. Different theoretical predictions are compared with the measurements, and ratios (R) between predictions and data are also shown. The RESBOS [62] prediction combines a next-to-leading order (NLO) fixed-order calculation at high Z boson p_T with the Collins-Soper-Sterman resummation formalism [66–68] at low boson p_T, which is an all-order summation of large terms from gluon emission. RESBOS is used to get predictions for all measurements, by generating a $Z \to \mu^+\mu^-$ sample using the CT18NNLO PDFs [37]. POWHEG-BOX [69–72] can be interfaced with PYTHIA for QCD showering. FEWZ [56] is a fixed-order generator for hadron collider production of lepton pairs through the Drell-Yan process at NNLO in the strong coupling constant. HERWIG [73, 74] with MATCHBOX mode is also used to get predictions, where MATCHBOX is a generator interfaced with higher-order corrections provided by HERWIG. As in the y^Z measurement the resummation effects are integrated, the measurements are compared with the predictions from a resummation calculation (RESBOS) and other higher-order calculations (FEWZ with CT14NNLO [34], NNPDF3.0NNLO [36], MMHT14NNLO [35] and ABM12NNLO [75], POWHEG, MATCHBOX with NNPDF3.1NLO [76], PYTHIA with CT09MCS [77], and $\alpha_s = 0.118$). Measurements are in good agreement with theoretical predictions. However, the FEWZ predictions for the ratios are systematically smaller than the measured results in the lower y^Z region, from 2.0 to 3.0. The ratio predicted by RESBOS using CT18NNLO is consistent with the meausred results. A consistency check has been performed, by fitting the measured differential cross-section of Z boson with the framework of the published W boson mass result [10], where the fitted α_S^Z from two analyses are consistent with each other within uncertainty.

The single differential cross-sections in regions of p_T^Z and ϕ_η^* are shown in figure 4 and figure 5, with ratios (R) of predictions to data are shown. Measurements are in reasonable agreement with the different theoretical predictions. In the lower p_T region, the measurements agree with predictions from RESBOS and PYTHIA with the LHCb tune [78], but disagree with other predictions. In the large p_T^Z and ϕ_η^* regions, the RESBOS predictions are in disagreement with the measured data. The POWHEG with PYTHIA prediction is larger than the measurements in the small p_T^Z region, and smaller in the middle and large p_T^Z region, indicating that the POWHEG prediction cannot describe the data. The predictions from MATCHBOX are smaller than the data in the first p_T^Z region, and larger than data in other p_T^Z regions. Similar conclusions are obtained for the predictions as a function of ϕ_η^*.

Thanks to the large size of the data sample, double differential cross-section measurements are performed in regions of y^Z and p_T^Z, and y^Z and ϕ_η^*. The measurements are compared with the RESBOS predictions in figure 6, with ratios (R) of predictions to data shown in figure 7, for $y^Z - p_T^Z$. The corresponding results for $y^Z - \phi_\eta^*$ are shown in figures 8 and 9. The RESBOS predictions are consistent with the measured results within the uncer-
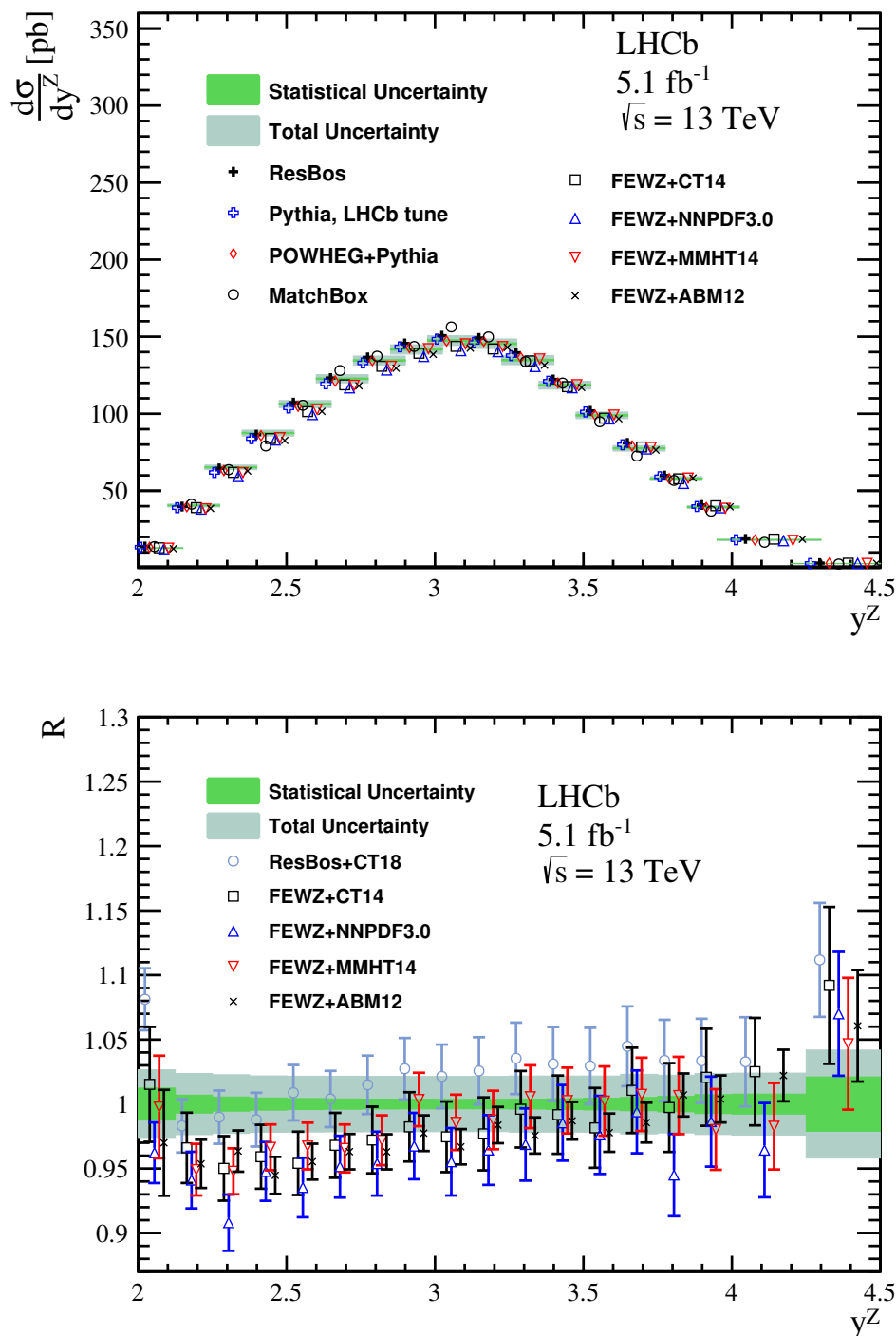
Figure 3. (Top) Measured single differential cross-section in regions of y^Z, compared with different theoretical predictions. In order to present the measurements more clearly, data bands are drawn wider than the width of the interval. (Bottom) Ratio of theoretical predictions to measured values, with the horizontal bars showing the uncertainty from the PDFs.
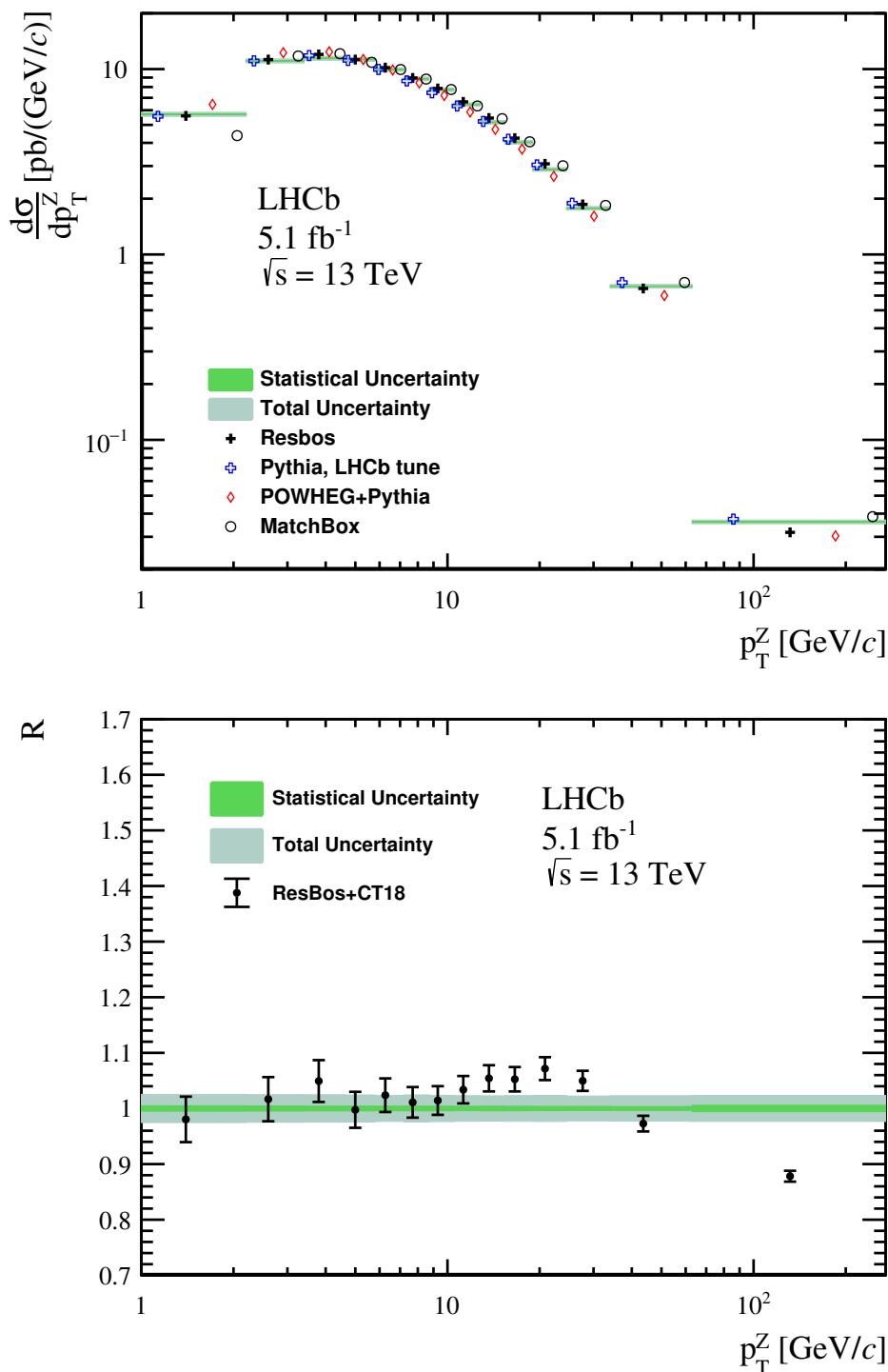
Figure 4. (Top) Measured single differential cross-section in regions of p_T^Z, compared with different theoretical predictions. (Bottom) Ratio of RESBOS predictions to measurement, with the horizontal bars showing the uncertainty from the PDFs.
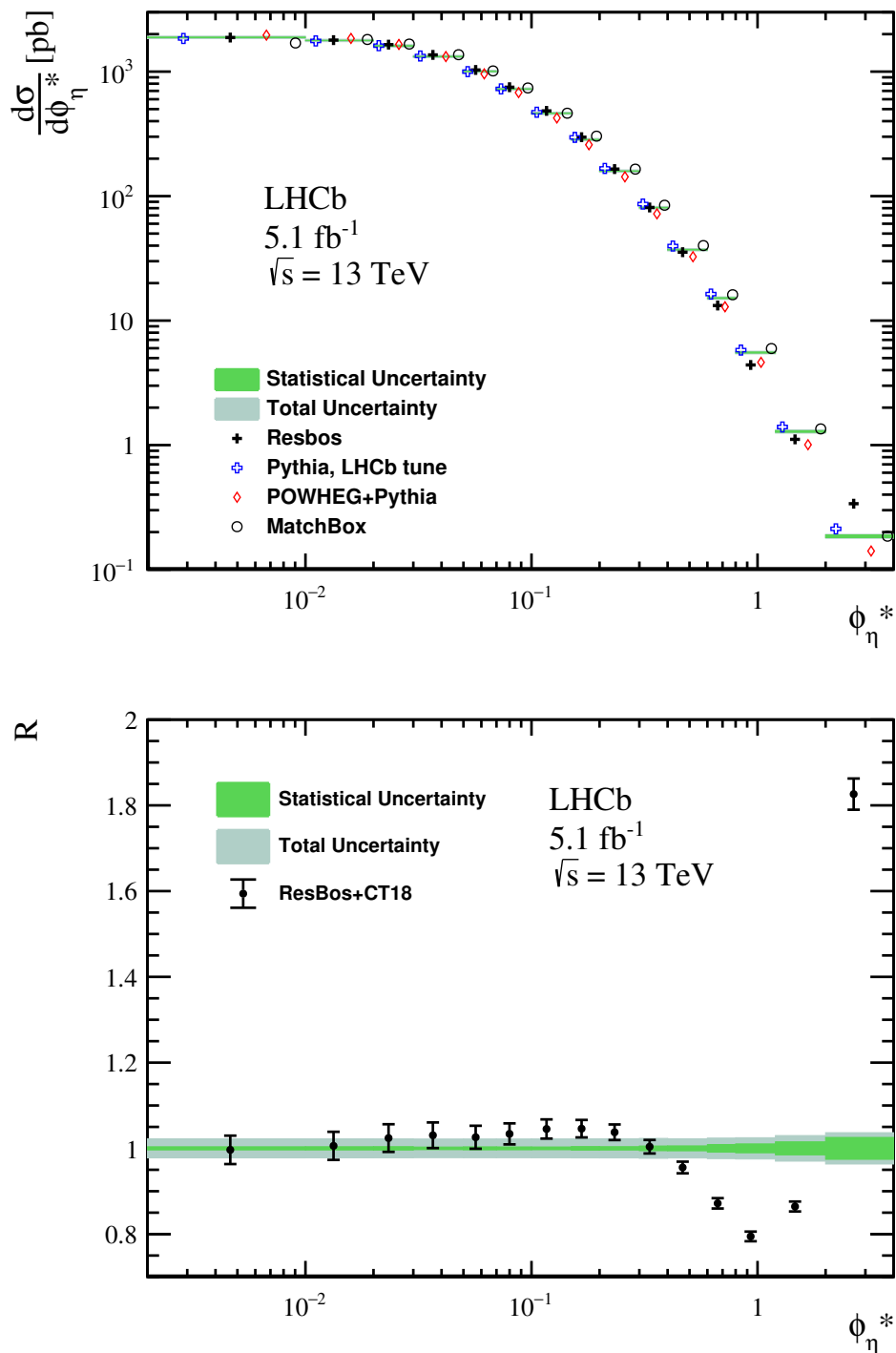
Figure 5. (Top) Measured single differential cross-section in regions of ϕ_η^*, compared with different theoretical predictions. (Bottom) Ratio of ResBos predictions to measurement, with the horizontal bars showing the uncertainty from the PDFs.
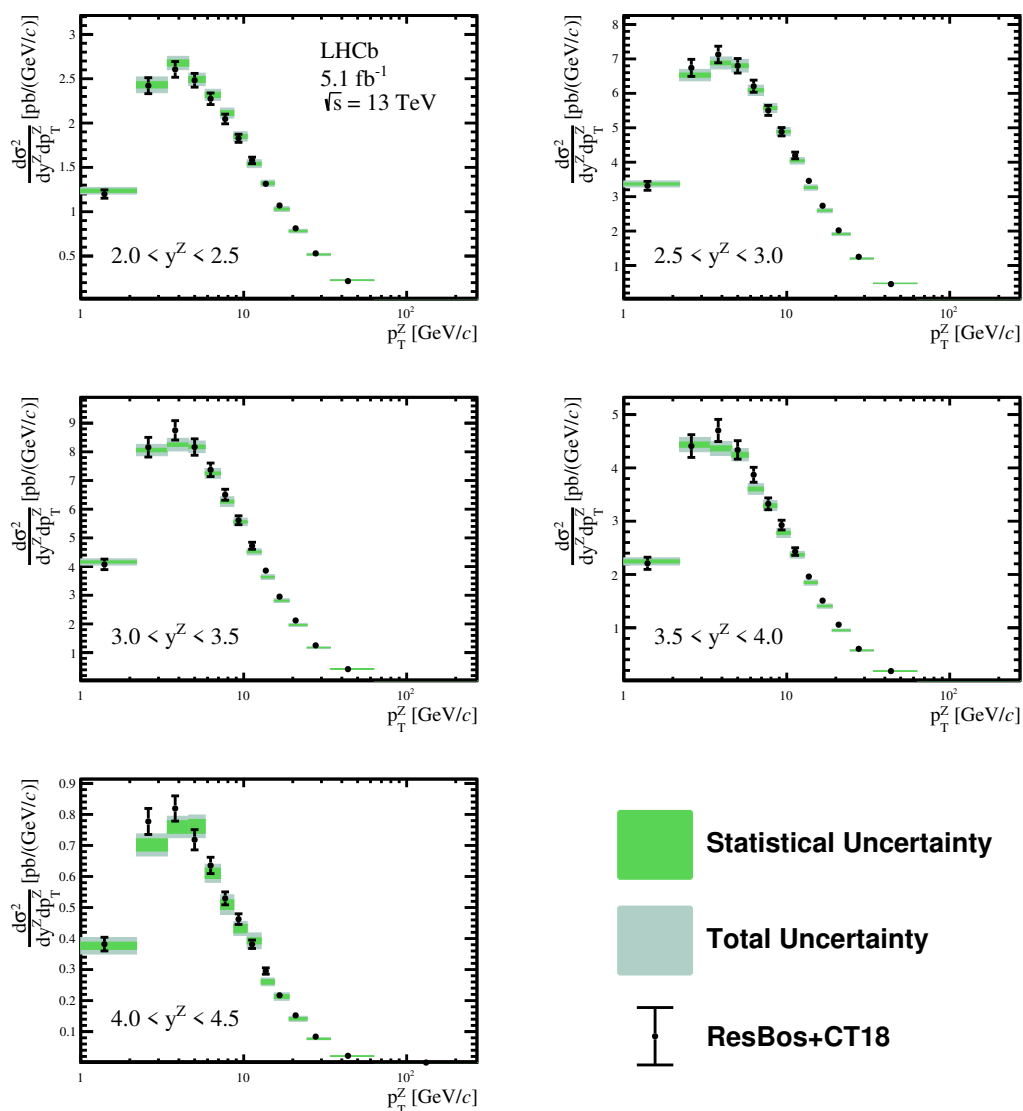
Figure 6. Measured double differential cross-section as a function of p_T^Z in regions of y^Z, compared with ResBos predictions, with the horizontal bars showing the uncertainty from the PDFs.

tainty. In the large p_T^Z and ϕ_η^* regions, there are sizable disagreements between data and predictions. Numerical results and systematic uncertainties are shown in appendix C.

7.2 Correlation matrices

The statistical correlation due to the event migration between regions is determined using simulation, where the numbers of signal events in different generator-level and reconstruction-level regions are used. The calculated correlation matrices are shown in appendix B. There are large correlations in the low p_T^Z region, and small correlations in the high p_T^Z region. On the other hand, the statistical correlation between regions in y^Z or in ϕ_η^* is found to be negligible.
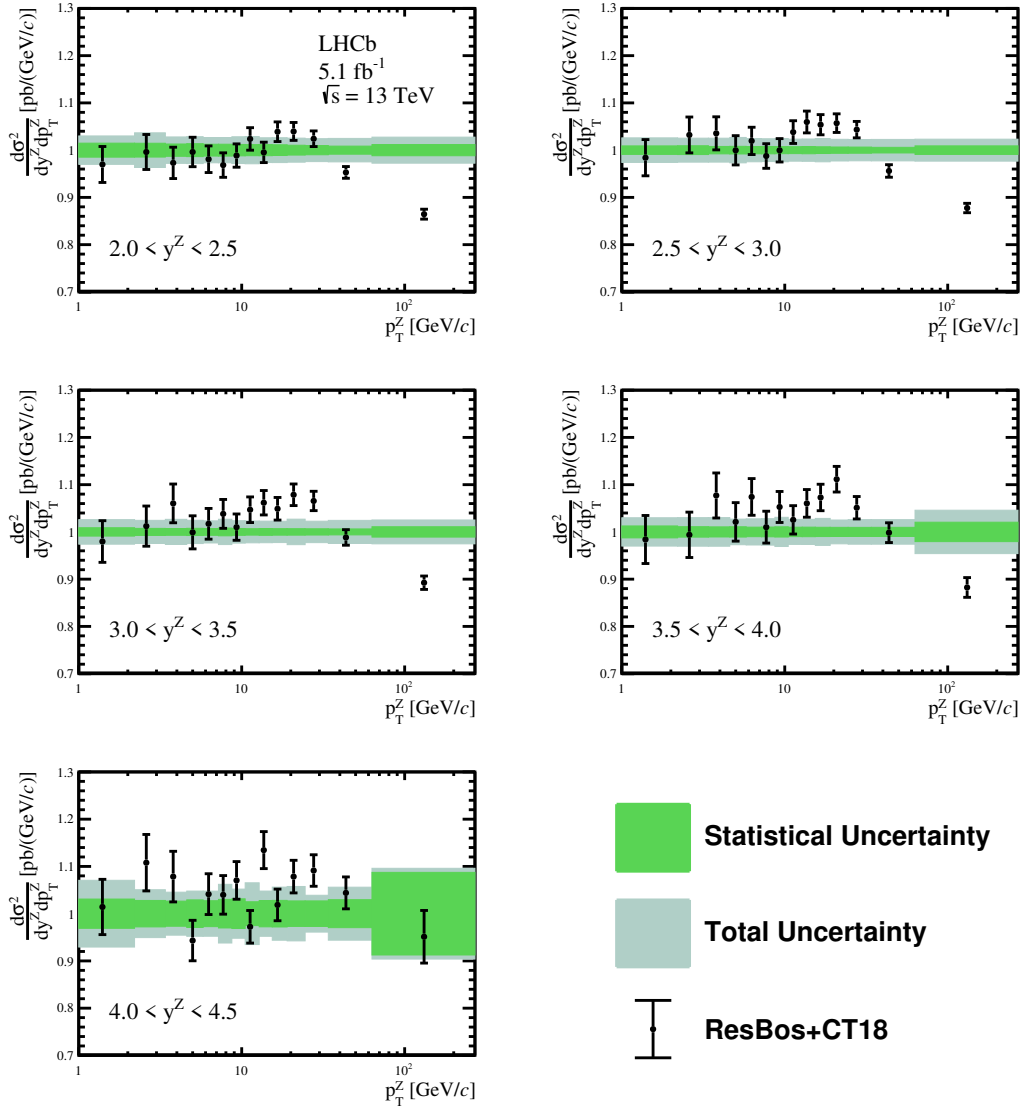
Figure 7. Ratios of RESBOS predictions to measurements as a function of p_T^Z in regions of y^Z, with the horizontal bars showing the uncertainty from the PDFs.

In the differential cross-section measurements, the systematic uncertainties from background, alignment, efficiency closure test, and FSR are considered to be 50% correlated between different regions. The luminosity uncertainty is considered to be 100% correlated between different regions. Regarding uncertainties from the selection efficiencies, the correlation between regions is determined by varying the efficiencies within their uncertainty, as

$$\text{cov}(f_k, f_l) = \sum_i \sum_j \left(\frac{\partial f_k}{\partial x_i}\right)\left(\frac{\partial f_l}{\partial x_j}\right) \cdot \text{cov}(x_i, x_j), \tag{7.1}$$

where $x_{i,j}$ is the determined efficiencies in i,j-th muon η region, $f_{k,l}$ is the measured Z boson cross-section with given efficiencies, and $\text{cov}(x_i, x_j)$ the correlation coefficient
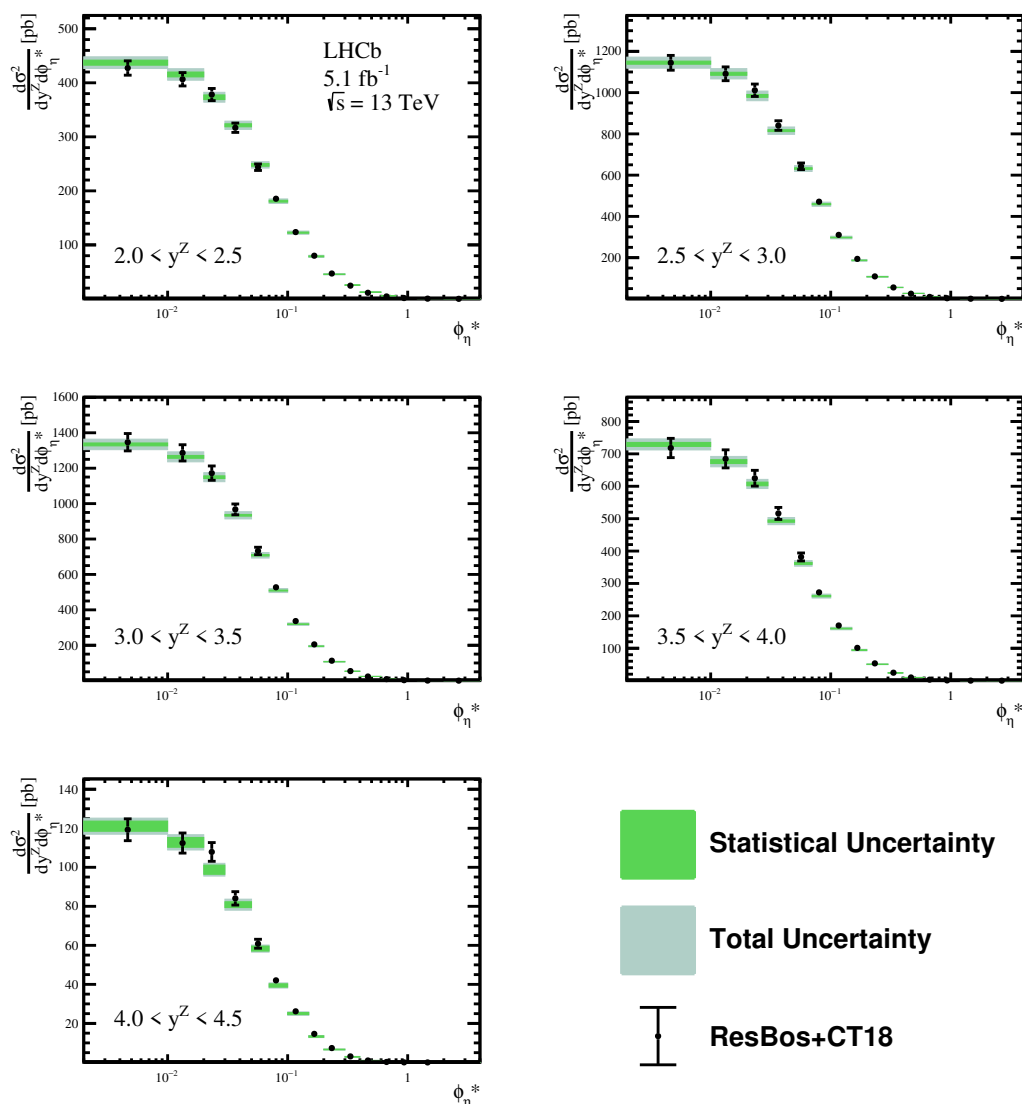
Figure 8. Measured double differential cross-section as a function of ϕ_η^* in regions of y^Z, compared with RESBOS predictions, with the horizontal bars showing the uncertainty from the PDFs.

between the i- and j-th region. The calculated correlation matrices for efficiencies are presented in appendix B. Because of the presence of two muons in the final state, there are large correlations between different regions in p_T^Z measurement. However, for the y^Z and ϕ_η^* measurements, small correlations are presented in most off-diagonal regions.

7.3 Integrated cross-section results

The measurements of integrated cross-section from different datasets are shown in appendix C. The χ^2 per degree-of-freedom of the combination is determined to be $0.9/2$, using the BLUE method.
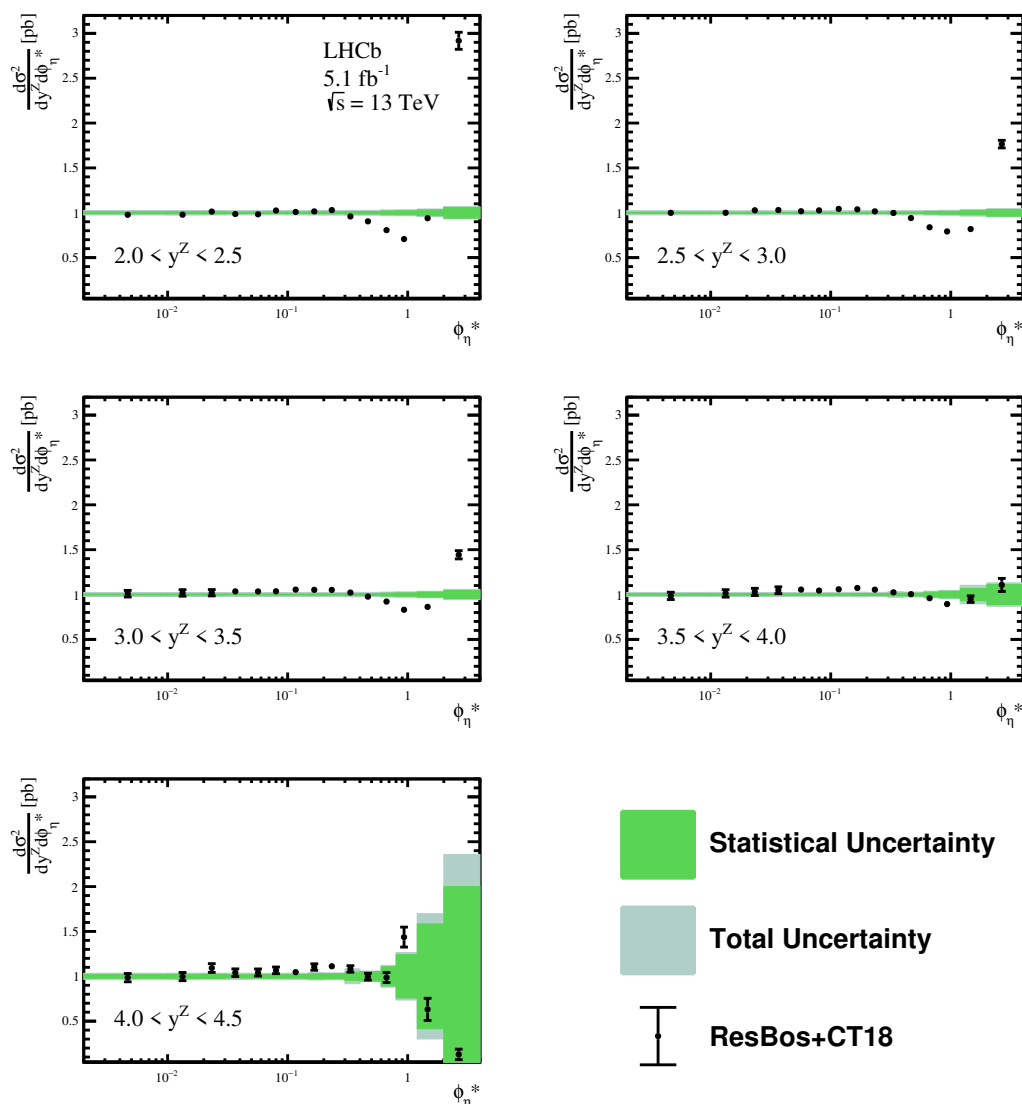
Figure 9. Ratios of RESBOS predictions to measurements as a function of ϕ_η^* in regions of y^Z, with the horizontal bars showing the uncertainty from the PDFs.

In the LHCb detector fiducial region, the Z boson integrated production cross-section is measured to be

$$\sigma(Z \to \mu^+\mu^-) = 196.4 \pm 0.2 \pm 1.6 \pm 3.9\,\text{pb},$$

where uncertainties are statistical, systematic, and due to the luminosity measurement, respectively. In figure 10 the determined integrated cross-section is compared with different theoretical predictions and the previous LHCb measurement [33]. In the comparison, the predictions are calculated using POWHEG with NNPDF3.1NLO [76], POWHEG with CT18NLO [37], RESBOS with CT18NNLO, FEWZ with CT14NNLO [34], FEWZ with NNPDF3.0NNLO [36], FEWZ with MMHT14NNLO [35], and FEWZ with
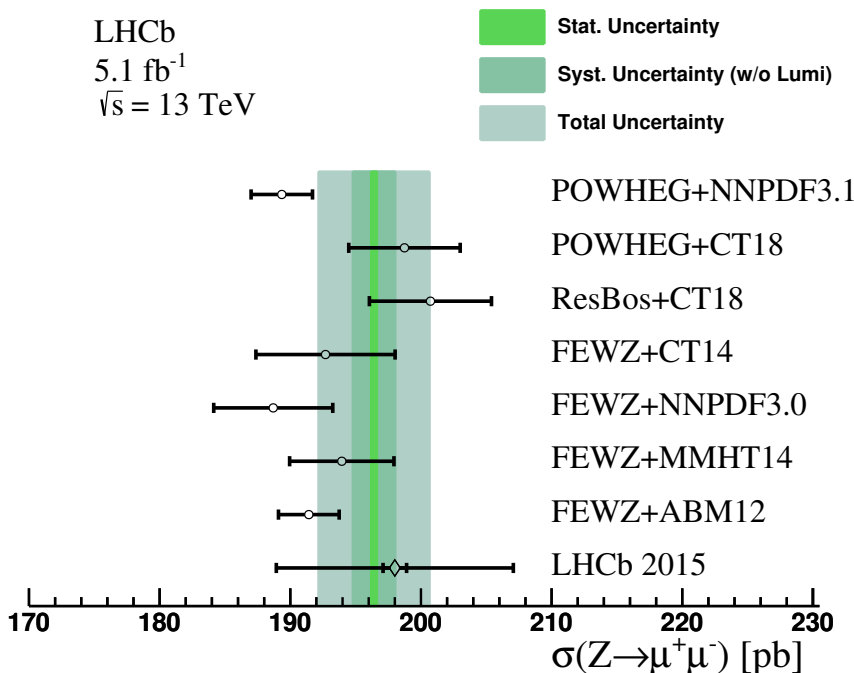
Figure 10. Comparison of the integrated cross-section, $\sigma_{Z\to\mu^+\mu^-}$, between data and theoretical predictions. The bands correspond to the data, with the inner band corresponding to the statistical uncertainty and the outer bands corresponding to the systematic uncertainty and total uncertainty. The open circles correspond to the different theoretical predictions. The diamond point corresponds to the previous LHCb measurement [33].

ABM12NNLO [75], with both their statistical and PDF uncertainties. Measurements are in reasonable agreement with all theoretical predictions.

8 Conclusion

In summary, the most precise measurement to date of the Z boson production cross-section in the forward region at $\sqrt{s} = 13\,\text{TeV}$ is presented, using pp collision data collected with the LHCb detector. The dataset corresponds to an integrated luminosity of $5.1 \pm 0.1\,\text{fb}^{-1}$. The integrated cross-section in fiducial region is measured to be

$$\sigma_{Z\to\mu^+\mu^-} = 196.4 \pm 0.2 \pm 1.6 \pm 3.9\,\text{pb},$$

where the first uncertainty is statistical, the second is systematic, and the third is due to the luminosity determination. The single differential and the double differential cross-sections are measured. This is the first measurement of the double differential cross-section in the forward region. Overall, reasonable agreement between measured results and the theoretical predictions are seen. However, there are sizable disagreements in the large p_T^Z and ϕ_η^* regions, which need more investigations in future. These measurements provide important and unique information to the PDF determination, especially in the large and small x regions.
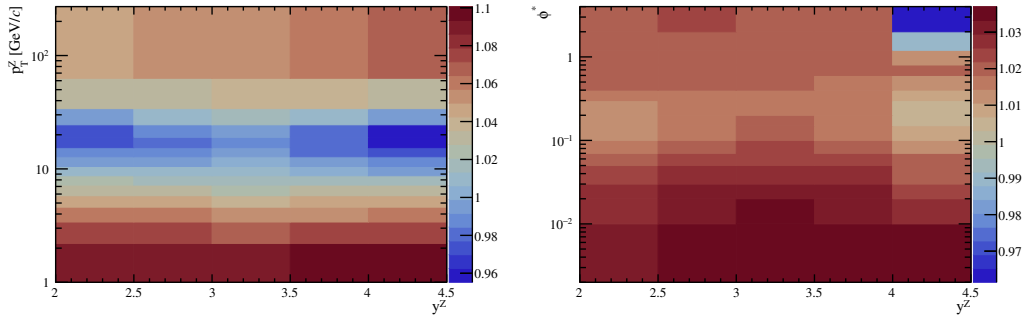
Figure 11. Final state radiation correction estimated for double differential cross section measurement for (left) $y^Z - p_T^Z$ measurement, and for (right) $y^Z - \phi_\eta^*$ measurement.

A Final state radiation corrections

Final state radiation corrections for double differential cross-section measurement are shown in figure 11. Tabled results of final state radiation corrections used in the single differential cross-section measurements are presented from table 2 to table 4. Final state radiation corrections used in the double differential cross-section measurements are presented in tables 5 and 6.

y^Z			Correction				
2.000	−	2.125	1.019	±	0.002	±	0.001
2.125	−	2.250	1.020	±	0.001	±	0.002
2.250	−	2.375	1.020	±	0.001	±	0.000
2.375	−	2.500	1.020	±	0.001	±	0.001
2.500	−	2.625	1.021	±	0.001	±	0.001
2.625	−	2.750	1.022	±	0.001	±	0.000
2.750	−	2.875	1.023	±	0.001	±	0.002
2.875	−	3.000	1.024	±	0.001	±	0.000
3.000	−	3.125	1.025	±	0.001	±	0.000
3.125	−	3.250	1.026	±	0.001	±	0.000
3.250	−	3.375	1.026	±	0.001	±	0.001
3.375	−	3.500	1.025	±	0.001	±	0.002
3.500	−	3.625	1.024	±	0.001	±	0.001
3.625	−	3.750	1.024	±	0.001	±	0.002
3.750	−	3.875	1.022	±	0.001	±	0.003
3.875	−	4.000	1.022	±	0.001	±	0.000
4.000	−	4.250	1.019	±	0.001	±	0.001
4.250	−	4.500	1.019	±	0.003	±	0.003

Table 2. Final state radiation correction used in the y^Z cross-section measurement. The first uncertainty is statistical and the second is systematic.

p_T^Z [GeV/c]			Correction				
0.0	−	2.2	1.091	±	0.001	±	0.000
2.2	−	3.4	1.072	±	0.001	±	0.009
3.4	−	4.6	1.057	±	0.001	±	0.002
4.6	−	5.8	1.043	±	0.001	±	0.001
5.8	−	7.2	1.030	±	0.001	±	0.001
7.2	−	8.7	1.018	±	0.001	±	0.008
8.7	−	10.5	1.007	±	0.001	±	0.006
10.5	−	12.8	0.996	±	0.001	±	0.005
12.8	−	15.4	0.988	±	0.001	±	0.003
15.4	−	19.0	0.983	±	0.001	±	0.006
19.0	−	24.5	0.987	±	0.001	±	0.007
24.5	−	34.0	1.010	±	0.001	±	0.001
34.0	−	63.0	1.034	±	0.001	±	0.000
63.0	−	270.0	1.053	±	0.001	±	0.004

Table 3. Final state radiation correction used in the p_T^Z cross-section measurement. The first uncertainty is statistical and the second is systematic.

	ϕ_η^*			Correction			
0.00	−	0.01	1.035	±	0.001	±	0.002
0.01	−	0.02	1.032	±	0.001	±	0.004
0.02	−	0.03	1.030	±	0.001	±	0.001
0.03	−	0.05	1.026	±	0.001	±	0.001
0.05	−	0.07	1.023	±	0.001	±	0.000
0.07	−	0.10	1.020	±	0.001	±	0.003
0.10	−	0.15	1.017	±	0.001	±	0.001
0.15	−	0.20	1.016	±	0.001	±	0.003
0.20	−	0.30	1.016	±	0.001	±	0.001
0.30	−	0.40	1.017	±	0.001	±	0.001
0.40	−	0.60	1.020	±	0.001	±	0.000
0.60	−	0.80	1.020	±	0.001	±	0.001
0.80	−	1.20	1.020	±	0.002	±	0.002
1.20	−	2.00	1.020	±	0.003	±	0.006
2.00	−	4.00	1.021	±	0.003	±	0.006

Table 4. Final state radiation correction used in the ϕ_η^* cross-section measurement. The first uncertainty is statistical and the second is systematic.

	y^Z			p_T^Z [GeV/c]			Correction			
2.0	−	2.5	0.0	−	2.2	1.092	±	0.002	±	0.007
2.0	−	2.5	2.2	−	3.4	1.074	±	0.002	±	0.023
2.0	−	2.5	3.4	−	4.6	1.060	±	0.002	±	0.008
2.0	−	2.5	4.6	−	5.8	1.045	±	0.002	±	0.000
2.0	−	2.5	5.8	−	7.2	1.033	±	0.002	±	0.004
2.0	−	2.5	7.2	−	8.7	1.021	±	0.002	±	0.003
2.0	−	2.5	8.7	−	10.5	1.010	±	0.002	±	0.004
2.0	−	2.5	10.5	−	12.8	0.995	±	0.002	±	0.014
2.0	−	2.5	12.8	−	15.4	0.986	±	0.002	±	0.007
2.0	−	2.5	15.4	−	19.0	0.976	±	0.002	±	0.005
2.0	−	2.5	19.0	−	24.5	0.977	±	0.002	±	0.003
2.0	−	2.5	24.5	−	34.0	0.998	±	0.002	±	0.001
2.0	−	2.5	34.0	−	63.0	1.028	±	0.001	±	0.003
2.0	−	2.5	63.0	−	270.0	1.049	±	0.003	±	0.007
2.5	−	3.0	0.0	−	2.2	1.090	±	0.001	±	0.001
2.5	−	3.0	2.2	−	3.4	1.072	±	0.001	±	0.006
2.5	−	3.0	3.4	−	4.6	1.057	±	0.001	±	0.002
2.5	−	3.0	4.6	−	5.8	1.044	±	0.001	±	0.004
2.5	−	3.0	5.8	−	7.2	1.031	±	0.001	±	0.000
2.5	−	3.0	7.2	−	8.7	1.018	±	0.001	±	0.003
2.5	−	3.0	8.7	−	10.5	1.007	±	0.001	±	0.009
2.5	−	3.0	10.5	−	12.8	0.997	±	0.001	±	0.001
2.5	−	3.0	12.8	−	15.4	0.987	±	0.001	±	0.003
2.5	−	3.0	15.4	−	19.0	0.984	±	0.001	±	0.009
2.5	−	3.0	19.0	−	24.5	0.988	±	0.001	±	0.005
2.5	−	3.0	24.5	−	34.0	1.011	±	0.001	±	0.001
2.5	−	3.0	34.0	−	63.0	1.034	±	0.001	±	0.002
2.5	−	3.0	63.0	−	270.0	1.052	±	0.002	±	0.001
3.0	−	3.5	0.0	−	2.2	1.089	±	0.001	±	0.002
3.0	−	3.5	2.2	−	3.4	1.069	±	0.001	±	0.006
3.0	−	3.5	3.4	−	4.6	1.055	±	0.001	±	0.010
3.0	−	3.5	4.6	−	5.8	1.041	±	0.001	±	0.002
3.0	−	3.5	5.8	−	7.2	1.028	±	0.001	±	0.002
3.0	−	3.5	7.2	−	8.7	1.019	±	0.001	±	0.012
3.0	−	3.5	8.7	−	10.5	1.008	±	0.001	±	0.003
3.0	−	3.5	10.5	−	12.8	0.999	±	0.001	±	0.005
3.0	−	3.5	12.8	−	15.4	0.993	±	0.001	±	0.003
3.0	−	3.5	15.4	−	19.0	0.989	±	0.001	±	0.002
3.0	−	3.5	19.0	−	24.5	0.995	±	0.001	±	0.012
3.0	−	3.5	24.5	−	34.0	1.015	±	0.001	±	0.002
3.0	−	3.5	34.0	−	63.0	1.037	±	0.001	±	0.001

	y^Z			p_T^Z [GeV/c]		Correction				
3.0	–	3.5	63.0	–	270.0	1.055	±	0.002	±	0.008
3.5	–	4.0	0.0	–	2.2	1.094	±	0.002	±	0.004
3.5	–	4.0	2.2	–	3.4	1.074	±	0.002	±	0.012
3.5	–	4.0	3.4	–	4.6	1.057	±	0.002	±	0.005
3.5	–	4.0	4.6	–	5.8	1.044	±	0.002	±	0.001
3.5	–	4.0	5.8	–	7.2	1.029	±	0.002	±	0.008
3.5	–	4.0	7.2	–	8.7	1.016	±	0.002	±	0.009
3.5	–	4.0	8.7	–	10.5	1.004	±	0.002	±	0.009
3.5	–	4.0	10.5	–	12.8	0.992	±	0.002	±	0.008
3.5	–	4.0	12.8	–	15.4	0.984	±	0.002	±	0.009
3.5	–	4.0	15.4	–	19.0	0.979	±	0.002	±	0.007
3.5	–	4.0	19.0	–	24.5	0.984	±	0.002	±	0.003
3.5	–	4.0	24.5	–	34.0	1.011	±	0.002	±	0.003
3.5	–	4.0	34.0	–	63.0	1.038	±	0.001	±	0.002
3.5	–	4.0	63.0	–	270.0	1.060	±	0.003	±	0.008
4.0	–	4.5	0.0	–	2.2	1.101	±	0.005	±	0.016
4.0	–	4.5	2.2	–	3.4	1.078	±	0.005	±	0.010
4.0	–	4.5	3.4	–	4.6	1.061	±	0.005	±	0.013
4.0	–	4.5	4.6	–	5.8	1.046	±	0.004	±	0.007
4.0	–	4.5	5.8	–	7.2	1.030	±	0.004	±	0.007
4.0	–	4.5	7.2	–	8.7	1.015	±	0.004	±	0.038
4.0	–	4.5	8.7	–	10.5	0.996	±	0.004	±	0.004
4.0	–	4.5	10.5	–	12.8	0.988	±	0.004	±	0.004
4.0	–	4.5	12.8	–	15.4	0.971	±	0.004	±	0.009
4.0	–	4.5	15.4	–	19.0	0.959	±	0.004	±	0.036
4.0	–	4.5	19.0	–	24.5	0.955	±	0.003	±	0.025
4.0	–	4.5	24.5	–	34.0	0.992	±	0.004	±	0.009
4.0	–	4.5	34.0	–	63.0	1.033	±	0.004	±	0.006
4.0	–	4.5	63.0	–	270.0	1.066	±	0.008	±	0.015

Table 5. Final state radiation correction used in the $y^Z - p_T^Z$ double cross-section measurement. The first uncertainty is statistical and the second is systematic.

	y^Z			ϕ_η^*		Correction				
2.0	–	2.5	0.00	–	0.01	1.030	±	0.002	±	0.000
2.0	–	2.5	0.01	–	0.02	1.028	±	0.002	±	0.005
2.0	–	2.5	0.02	–	0.03	1.026	±	0.002	±	0.004
2.0	–	2.5	0.03	–	0.05	1.024	±	0.001	±	0.002
2.0	–	2.5	0.05	–	0.07	1.019	±	0.002	±	0.003
2.0	–	2.5	0.07	–	0.10	1.017	±	0.001	±	0.003
2.0	–	2.5	0.10	–	0.15	1.014	±	0.001	±	0.000

	y^Z			ϕ^*_η		Correction				
2.0	−	2.5	0.15	−	0.20	1.013	±	0.002	±	0.005
2.0	−	2.5	0.20	−	0.30	1.014	±	0.002	±	0.003
2.0	−	2.5	0.30	−	0.40	1.017	±	0.002	±	0.004
2.0	−	2.5	0.40	−	0.60	1.019	±	0.002	±	0.002
2.0	−	2.5	0.60	−	0.80	1.018	±	0.004	±	0.009
2.0	−	2.5	0.80	−	1.20	1.019	±	0.005	±	0.002
2.0	−	2.5	1.20	−	2.00	1.018	±	0.007	±	0.015
2.0	−	2.5	2.00	−	4.00	1.019	±	0.006	±	0.005
2.5	−	3.0	0.00	−	0.01	1.034	±	0.001	±	0.004
2.5	−	3.0	0.01	−	0.02	1.031	±	0.001	±	0.005
2.5	−	3.0	0.02	−	0.03	1.030	±	0.001	±	0.003
2.5	−	3.0	0.03	−	0.05	1.026	±	0.001	±	0.002
2.5	−	3.0	0.05	−	0.07	1.022	±	0.001	±	0.002
2.5	−	3.0	0.07	−	0.10	1.019	±	0.001	±	0.001
2.5	−	3.0	0.10	−	0.15	1.017	±	0.001	±	0.001
2.5	−	3.0	0.15	−	0.20	1.017	±	0.001	±	0.004
2.5	−	3.0	0.20	−	0.30	1.016	±	0.001	±	0.001
2.5	−	3.0	0.30	−	0.40	1.018	±	0.001	±	0.002
2.5	−	3.0	0.40	−	0.60	1.020	±	0.002	±	0.003
2.5	−	3.0	0.60	−	0.80	1.020	±	0.002	±	0.000
2.5	−	3.0	0.80	−	1.20	1.020	±	0.003	±	0.005
2.5	−	3.0	1.20	−	2.00	1.021	±	0.004	±	0.020
2.5	−	3.0	2.00	−	4.00	1.022	±	0.005	±	0.004
3.0	−	3.5	0.00	−	0.01	1.037	±	0.001	±	0.001
3.0	−	3.5	0.01	−	0.02	1.035	±	0.001	±	0.001
3.0	−	3.5	0.02	−	0.03	1.033	±	0.001	±	0.001
3.0	−	3.5	0.03	−	0.05	1.028	±	0.001	±	0.002
3.0	−	3.5	0.05	−	0.07	1.025	±	0.001	±	0.003
3.0	−	3.5	0.07	−	0.10	1.022	±	0.001	±	0.004
3.0	−	3.5	0.10	−	0.15	1.019	±	0.001	±	0.000
3.0	−	3.5	0.15	−	0.20	1.018	±	0.001	±	0.002
3.0	−	3.5	0.20	−	0.30	1.017	±	0.001	±	0.005
3.0	−	3.5	0.30	−	0.40	1.017	±	0.001	±	0.001
3.0	−	3.5	0.40	−	0.60	1.021	±	0.002	±	0.004
3.0	−	3.5	0.60	−	0.80	1.021	±	0.002	±	0.005
3.0	−	3.5	0.80	−	1.20	1.021	±	0.003	±	0.001
3.0	−	3.5	1.20	−	2.00	1.019	±	0.005	±	0.004
3.0	−	3.5	2.00	−	4.00	1.022	±	0.006	±	0.026
3.5	−	4.0	0.00	−	0.01	1.034	±	0.002	±	0.004

y^Z			ϕ_η^*			Correction				
3.5	−	4.0	0.01	−	0.02	1.033	±	0.002	±	0.004
3.5	−	4.0	0.02	−	0.03	1.030	±	0.002	±	0.001
3.5	−	4.0	0.03	−	0.05	1.026	±	0.001	±	0.001
3.5	−	4.0	0.05	−	0.07	1.022	±	0.001	±	0.002
3.5	−	4.0	0.07	−	0.10	1.019	±	0.001	±	0.004
3.5	−	4.0	0.10	−	0.15	1.016	±	0.001	±	0.003
3.5	−	4.0	0.15	−	0.20	1.015	±	0.002	±	0.002
3.5	−	4.0	0.20	−	0.30	1.015	±	0.002	±	0.005
3.5	−	4.0	0.30	−	0.40	1.016	±	0.002	±	0.001
3.5	−	4.0	0.40	−	0.60	1.018	±	0.002	±	0.002
3.5	−	4.0	0.60	−	0.80	1.020	±	0.004	±	0.007
3.5	−	4.0	0.80	−	1.20	1.021	±	0.005	±	0.003
3.5	−	4.0	1.20	−	2.00	1.020	±	0.009	±	0.020
3.5	−	4.0	2.00	−	4.00	1.018	±	0.016	±	0.018
4.0	−	4.5	0.00	−	0.01	1.035	±	0.004	±	0.002
4.0	−	4.5	0.01	−	0.02	1.029	±	0.004	±	0.016
4.0	−	4.5	0.02	−	0.03	1.024	±	0.004	±	0.002
4.0	−	4.5	0.03	−	0.05	1.021	±	0.003	±	0.004
4.0	−	4.5	0.05	−	0.07	1.020	±	0.003	±	0.006
4.0	−	4.5	0.07	−	0.10	1.014	±	0.003	±	0.007
4.0	−	4.5	0.10	−	0.15	1.009	±	0.003	±	0.004
4.0	−	4.5	0.15	−	0.20	1.005	±	0.004	±	0.016
4.0	−	4.5	0.20	−	0.30	1.007	±	0.004	±	0.009
4.0	−	4.5	0.30	−	0.40	1.007	±	0.005	±	0.011
4.0	−	4.5	0.40	−	0.60	1.013	±	0.006	±	0.008
4.0	−	4.5	0.60	−	0.80	1.019	±	0.010	±	0.001
4.0	−	4.5	0.80	−	1.20	1.011	±	0.017	±	0.075
4.0	−	4.5	1.20	−	2.00	0.988	±	0.037	±	0.238
4.0	−	4.5	2.00	−	4.00	0.961	±	0.134	±	0.039

Table 6. Final state radiation correction used in the $y^Z - \phi_\eta^*$ double cross-section measurement. The first uncertainty is statistical and the second is systematic.

B   Correlation matrices

The calculated correlation matrices for statistical uncertainty are shown in figures 12 and 13, and presented from table 7 to 9, and the correlation matrices for efficiency uncertainty are shown in figures 14 and 15 for single and double differential cross-section measurements, and presented from table 10 to 12.
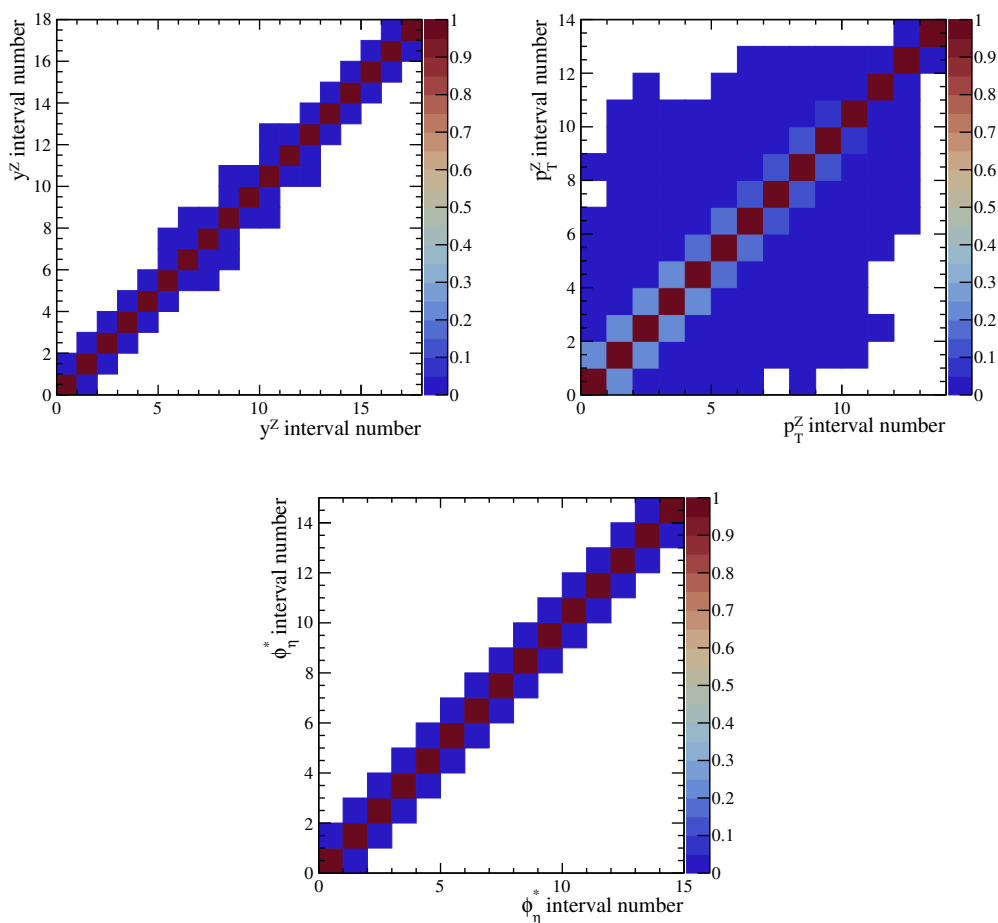
Figure 12. Statistical correlation matrix of the cross-section measurements in one-dimensional interval regions of (top-left) y^Z, (top-right) p_T^Z and (bottom) ϕ_η^*. More details about the 'interval number' can be found from table 14 and table 16.
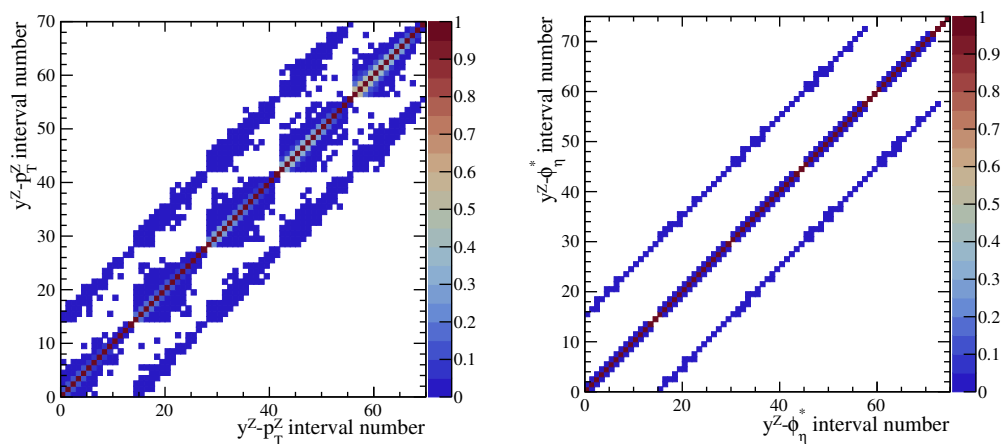
Figure 13. Statistical correlation matrix of the cross-section measurements in two-dimensional interval regions of (left) $y^Z - p_T^Z$ and (right) $y^Z - \phi_\eta^*$. More details about the 'interval number' can be found in table 17 and table 18.

Interval	1	2	3	4	5	6	7	8	9	10	11	12	13	14	15	16	17	18
1	1.00																	
2	0.00	1.00																
3	0.00	0.00	1.00															
4	0.00	0.00	0.00	1.00														
5	0.00	0.00	0.00	0.01	1.00													
6	0.00	0.00	0.00	0.00	0.01	1.00												
7	0.00	0.00	0.00	0.00	0.00	0.01	1.00											
8	0.00	0.00	0.00	0.00	0.00	0.00	0.01	1.00										
9	0.00	0.00	0.00	0.00	0.00	0.00	0.00	0.01	1.00									
10	0.00	0.00	0.00	0.00	0.00	0.00	0.00	0.00	0.02	1.00								
11	0.00	0.00	0.00	0.00	0.00	0.00	0.00	0.00	0.00	0.02	1.00							
12	0.00	0.00	0.00	0.00	0.00	0.00	0.00	0.00	0.00	0.00	0.02	1.00						
13	0.00	0.00	0.00	0.00	0.00	0.00	0.00	0.00	0.00	0.00	0.00	0.02	1.00					
14	0.00	0.00	0.00	0.00	0.00	0.00	0.00	0.00	0.00	0.00	0.00	0.00	0.02	1.00				
15	0.00	0.00	0.00	0.00	0.00	0.00	0.00	0.00	0.00	0.00	0.00	0.00	0.00	0.02	1.00			
16	0.00	0.00	0.00	0.00	0.00	0.00	0.00	0.00	0.00	0.00	0.00	0.00	0.00	0.00	0.02	1.00		
17	0.00	0.00	0.00	0.00	0.00	0.00	0.00	0.00	0.00	0.00	0.00	0.00	0.00	0.00	0.00	0.01	1.00	
18	0.00	0.00	0.00	0.00	0.00	0.00	0.00	0.00	0.00	0.00	0.00	0.00	0.00	0.00	0.00	0.00	0.00	1.00

Table 7. Correlation matrix of statistical uncertainty for one-dimensional y^Z measurement.

Interval	1	2	3	4	5	6	7	8	9	10	11	12	13	14
1	1.00													
2	0.22	1.00												
3	0.03	0.24	1.00											
4	0.00	0.02	0.22	1.00										
5	0.00	0.00	0.02	0.22	1.00									
6	0.00	0.00	0.00	0.02	0.19	1.00								
7	0.00	0.00	0.00	0.00	0.01	0.18	1.00							
8	0.00	0.00	0.00	0.00	0.00	0.01	0.15	1.00						
9	0.00	0.00	0.00	0.00	0.00	0.00	0.00	0.11	1.00					
10	0.00	0.00	0.00	0.00	0.00	0.00	0.00	0.00	0.11	1.00				
11	0.00	0.00	0.00	0.00	0.00	0.00	0.00	0.00	0.00	0.08	1.00			
12	0.00	0.00	0.00	0.00	0.00	0.00	0.00	0.00	0.00	0.00	0.05	1.00		
13	0.00	0.00	0.00	0.00	0.00	0.00	0.00	0.00	0.00	0.00	0.00	0.03	1.00	
14	0.00	0.00	0.00	0.00	0.00	0.00	0.00	0.00	0.00	0.00	0.00	0.00	0.01	1.00

Table 8. Correlation matrix of statistical uncertainty for one-dimensional p_T^Z measurement.

Interval	1	2	3	4	5	6	7	8	9	10	11	12	13	14	15
1	1.00														
2	0.01	1.00													
3	0.00	0.01	1.00												
4	0.00	0.00	0.01	1.00											
5	0.00	0.00	0.00	0.00	1.00										
6	0.00	0.00	0.00	0.00	0.00	1.00									
7	0.00	0.00	0.00	0.00	0.00	0.00	1.00								
8	0.00	0.00	0.00	0.00	0.00	0.00	0.00	1.00							
9	0.00	0.00	0.00	0.00	0.00	0.00	0.00	0.00	1.00						
10	0.00	0.00	0.00	0.00	0.00	0.00	0.00	0.00	0.00	1.00					
11	0.00	0.00	0.00	0.00	0.00	0.00	0.00	0.00	0.00	0.00	1.00				
12	0.00	0.00	0.00	0.00	0.00	0.00	0.00	0.00	0.00	0.00	0.00	1.00			
13	0.00	0.00	0.00	0.00	0.00	0.00	0.00	0.00	0.00	0.00	0.00	0.00	1.00		
14	0.00	0.00	0.00	0.00	0.00	0.00	0.00	0.00	0.00	0.00	0.00	0.00	0.00	1.00	
15	0.00	0.00	0.00	0.00	0.00	0.00	0.00	0.00	0.00	0.00	0.00	0.00	0.00	0.00	1.00

Table 9. Correlation matrix of statistical uncertainty for one-dimensional ϕ_η^* measurement.
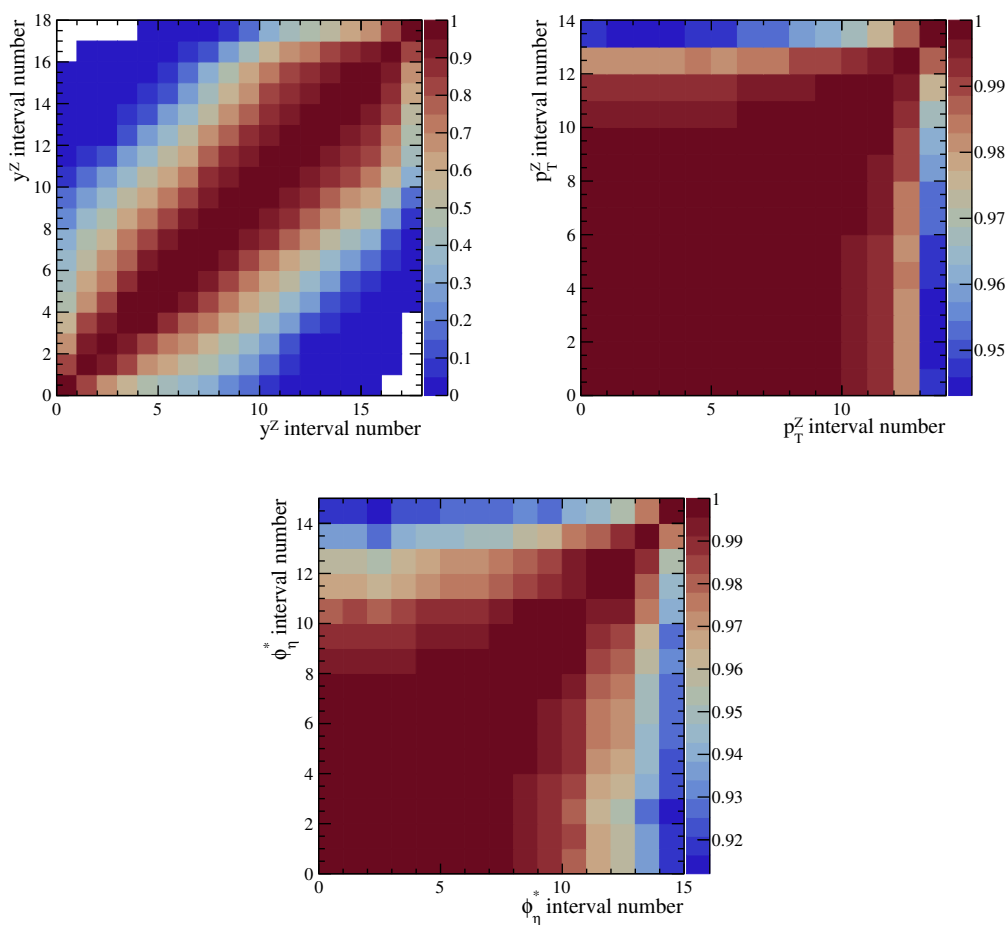
Figure 14. Correlation matrix of efficiencies uncertainty for one-dimensional (top-left) y^Z, (top-right) p_T^Z and (bottom) ϕ_η^* measurements. More details about the 'interval number' can be found in table 14 and table 16.
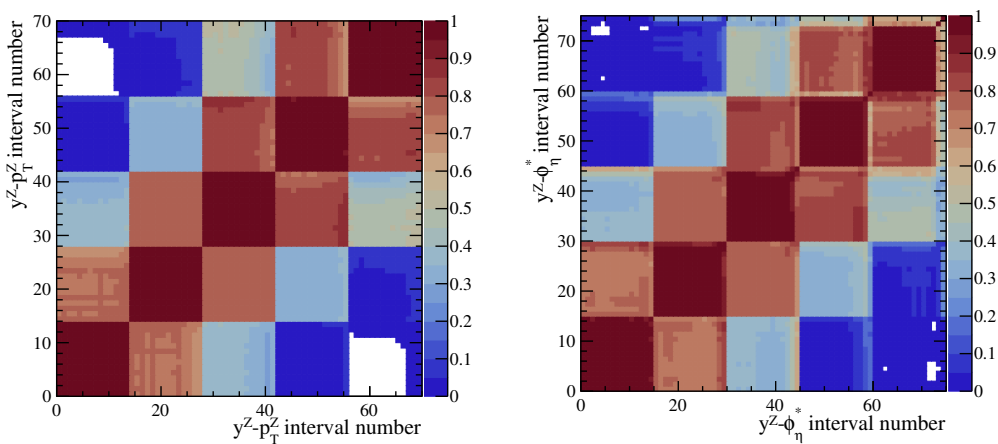
Figure 15. Correlation matrix of efficiencies uncertainty for two-dimensional (left) $y^Z - p_T^Z$ and (right) $y^Z - \phi_\eta^*$ measurements. More details about the 'interval number' can be found in table 17 and table 18.

Interval	1	2	3	4	5	6	7	8	9	10	11	12	13	14	15	16	17	18
1	1.00																	
2	0.84	1.00																
3	0.67	0.92	1.00															
4	0.57	0.81	0.95	1.00														
5	0.49	0.70	0.84	0.95	1.00													
6	0.43	0.62	0.75	0.87	0.97	1.00												
7	0.37	0.55	0.67	0.79	0.91	0.98	1.00											
8	0.31	0.47	0.59	0.71	0.83	0.91	0.97	1.00										
9	0.25	0.38	0.49	0.62	0.74	0.83	0.92	0.98	1.00									
10	0.17	0.29	0.40	0.51	0.64	0.74	0.84	0.93	0.98	1.00								
11	0.09	0.18	0.28	0.39	0.53	0.63	0.75	0.85	0.93	0.98	1.00							
12	0.02	0.06	0.14	0.25	0.39	0.50	0.63	0.75	0.85	0.93	0.98	1.00						
13	0.00	0.01	0.05	0.13	0.26	0.38	0.52	0.65	0.77	0.87	0.95	0.99	1.00					
14	0.00	0.00	0.01	0.06	0.15	0.26	0.40	0.55	0.68	0.80	0.89	0.95	0.98	1.00				
15	0.00	0.00	0.00	0.02	0.06	0.14	0.27	0.42	0.57	0.70	0.81	0.88	0.93	0.98	1.00			
16	0.00	0.00	0.00	0.00	0.02	0.06	0.16	0.31	0.46	0.60	0.73	0.81	0.87	0.93	0.98	1.00		
17	0.00	0.00	0.00	0.00	0.00	0.01	0.05	0.14	0.28	0.43	0.57	0.66	0.73	0.80	0.87	0.93	1.00	
18	0.00	0.00	0.00	0.00	0.00	0.00	0.00	0.01	0.07	0.19	0.33	0.42	0.48	0.55	0.62	0.69	0.85	1.00

Table 10. Correlation matrix of efficiency uncertainty for one-dimensional y^Z measurement.

Interval	1	2	3	4	5	6	7	8	9	10	11	12	13	14
1	1.00													
2	1.00	1.00												
3	1.00	1.00	1.00											
4	1.00	1.00	1.00	1.00										
5	1.00	1.00	1.00	1.00	1.00									
6	1.00	1.00	1.00	1.00	1.00	1.00								
7	1.00	1.00	1.00	1.00	1.00	1.00	1.00							
8	1.00	1.00	1.00	1.00	1.00	1.00	1.00	1.00						
9	1.00	1.00	1.00	1.00	1.00	1.00	1.00	1.00	1.00					
10	1.00	1.00	1.00	1.00	1.00	1.00	1.00	1.00	1.00	1.00				
11	1.00	1.00	1.00	1.00	1.00	1.00	1.00	1.00	1.00	1.00	1.00			
12	0.99	0.99	0.99	0.99	0.99	0.99	0.99	0.99	1.00	1.00	1.00	1.00		
13	0.98	0.98	0.98	0.98	0.98	0.98	0.99	0.99	0.99	0.99	0.99	1.00	1.00	
14	0.95	0.94	0.94	0.95	0.95	0.95	0.95	0.95	0.96	0.96	0.97	0.98	0.99	1.00

Table 11. Correlation matrix of efficiency uncertainty for one-dimensional p_T^Z measurement.

Interval	1	2	3	4	5	6	7	8	9	10	11	12	13	14	15
1	1.00														
2	1.00	1.00													
3	1.00	1.00	1.00												
4	1.00	1.00	1.00	1.00											
5	1.00	1.00	1.00	1.00	1.00										
6	1.00	1.00	1.00	1.00	1.00	1.00									
7	1.00	1.00	1.00	1.00	1.00	1.00	1.00								
8	1.00	1.00	1.00	1.00	1.00	1.00	1.00	1.00							
9	0.99	0.99	0.99	1.00	1.00	1.00	1.00	1.00	1.00						
10	0.99	0.99	0.99	0.99	0.99	1.00	1.00	1.00	1.00	1.00					
11	0.98	0.98	0.98	0.98	0.99	0.99	0.99	0.99	1.00	1.00	1.00				
12	0.97	0.97	0.96	0.97	0.97	0.97	0.98	0.98	0.99	0.99	1.00	1.00			
13	0.96	0.96	0.96	0.96	0.97	0.97	0.97	0.98	0.98	0.99	0.99	1.00	1.00		
14	0.93	0.93	0.93	0.94	0.94	0.95	0.95	0.95	0.96	0.96	0.98	0.98	0.99	1.00	
15	0.92	0.92	0.91	0.92	0.92	0.93	0.93	0.93	0.93	0.93	0.94	0.94	0.95	0.98	1.00

Table 12. Correlation matrix of efficiency uncertainty for one-dimensional ϕ^*_η measurement.

Year	$\sigma(Z \to \mu^+\mu^-)$ [pb]
2016	$195.0 \pm 0.4 \pm 2.0 \pm 3.9$
2017	$197.0 \pm 0.4 \pm 1.9 \pm 3.9$
2018	$197.3 \pm 0.4 \pm 1.9 \pm 3.9$
Run II	$196.4 \pm 0.2 \pm 1.6 \pm 3.9$

Table 13. Measured total Z-boson cross-section for different datasets. The first uncertainty is statistical, the second systematic, and the third is due to the luminosity.

y^{Z}			$d\sigma(Z \to \mu^+\mu^-)/dy^{\mathrm{Z}}$ [pb]						
2.000	$-$	2.125	12.8	$\pm$	0.2	$\pm$	0.2	$\pm$	0.3
2.125	$-$	2.250	40.4	$\pm$	0.3	$\pm$	0.4	$\pm$	0.8
2.250	$-$	2.375	65.2	$\pm$	0.4	$\pm$	0.6	$\pm$	1.3
2.375	$-$	2.500	87.5	$\pm$	0.4	$\pm$	0.6	$\pm$	1.7
2.500	$-$	2.625	106.3	$\pm$	0.5	$\pm$	0.8	$\pm$	2.1
2.625	$-$	2.750	122.7	$\pm$	0.5	$\pm$	0.9	$\pm$	2.5
2.750	$-$	2.875	134.5	$\pm$	0.5	$\pm$	0.9	$\pm$	2.7
2.875	$-$	3.000	141.7	$\pm$	0.5	$\pm$	0.9	$\pm$	2.8
3.000	$-$	3.125	147.5	$\pm$	0.5	$\pm$	1.0	$\pm$	2.9
3.125	$-$	3.250	145.4	$\pm$	0.5	$\pm$	1.0	$\pm$	2.9
3.250	$-$	3.375	134.8	$\pm$	0.5	$\pm$	1.0	$\pm$	2.7
3.375	$-$	3.500	118.5	$\pm$	0.5	$\pm$	0.9	$\pm$	2.4
3.500	$-$	3.625	99.0	$\pm$	0.4	$\pm$	0.7	$\pm$	2.0
3.625	$-$	3.750	77.6	$\pm$	0.4	$\pm$	0.8	$\pm$	1.6
3.750	$-$	3.875	57.9	$\pm$	0.3	$\pm$	0.5	$\pm$	1.2
3.875	$-$	4.000	39.5	$\pm$	0.3	$\pm$	0.4	$\pm$	0.8
4.000	$-$	4.250	18.2	$\pm$	0.1	$\pm$	0.2	$\pm$	0.4
4.250	$-$	4.500	2.7	$\pm$	0.1	$\pm$	0.1	$\pm$	0.1

Table 14. Measured single differential cross-sections in interval regions of y^{Z}. The first uncertainty is statistical, the second systematic, and the third is due to the luminosity.

C Numerical results

The measured total cross-sections using different data sets are presented in table 13. The measured single differential cross-sections in interval regions of y^{Z}, p_{T}^Z and ϕ_η^* are presented from table 14 to 16. The measured double differential cross-section as a function of p_{T}^Z and ϕ_η^* in interval regions of y^{Z} are presented in tables 17 and 18.

The summarized systematic uncertainties for single differential cross-sections are shown in table 19 to 21, and in tables 22 and 23 for double differential cross-section measurements.

p_{T}^{Z} [GeV/c]			$d\sigma(Z \to \mu^{+}\mu^{-})/dp_{\mathrm{T}}^{Z}$ [pb]					
0.0	−	2.2	5.70	±	0.03	±	0.08	±	0.11
2.2	−	3.4	11.07	±	0.05	±	0.16	±	0.22
3.4	−	4.6	11.44	±	0.05	±	0.16	±	0.23
4.6	−	5.8	11.28	±	0.05	±	0.15	±	0.23
5.8	−	7.2	9.94	±	0.04	±	0.11	±	0.20
7.2	−	8.7	8.86	±	0.04	±	0.12	±	0.18
8.7	−	10.5	7.75	±	0.03	±	0.09	±	0.15
10.5	−	12.8	6.44	±	0.03	±	0.07	±	0.13
12.8	−	15.4	5.16	±	0.02	±	0.05	±	0.10
15.4	−	19.0	4.03	±	0.02	±	0.04	±	0.08
19.0	−	24.5	2.88	±	0.01	±	0.03	±	0.06
24.5	−	34.0	1.774	±	0.007	±	0.016	±	0.035
34.0	−	63.0	0.674	±	0.002	±	0.007	±	0.013
63.0	−	270.0	0.0361	±	0.0002	±	0.0004	±	0.0007

Table 15. Measured single differential cross-sections in interval regions of p_{T}^{Z}. The first uncertainty is statistical, the second systematic, and the third is due to the luminosity.

ϕ_{η}^{*}			$d\sigma(Z \to \mu^{+}\mu^{-})/d\phi_{\eta}^{*}$ [pb]					
0.00	−	0.01	1885	±	7	±	17	±	38
0.01	−	0.02	1780	±	7	±	16	±	36
0.02	−	0.03	1609	±	6	±	14	±	32
0.03	−	0.05	1322	±	4	±	11	±	26
0.05	−	0.07	1005	±	4	±	8	±	20
0.07	−	0.10	724.9	±	2.5	±	6.0	±	14.5
0.10	−	0.15	462.8	±	1.5	±	4.0	±	9.3
0.15	−	0.20	284.4	±	1.2	±	2.5	±	5.7
0.20	−	0.30	158.9	±	0.6	±	1.4	±	3.2
0.30	−	0.40	80.73	±	0.44	±	0.84	±	1.61
0.40	−	0.60	37.10	±	0.21	±	0.32	±	0.74
0.60	−	0.80	15.16	±	0.14	±	0.15	±	0.30
0.80	−	1.20	5.54	±	0.06	±	0.06	±	0.11
1.20	−	2.00	1.286	±	0.020	±	0.021	±	0.026
2.00	−	4.00	0.185	±	0.005	±	0.003	±	0.004

Table 16. Measured single differential cross-sections in interval regions of ϕ_{η}^{*}. The first uncertainty is statistical, the second systematic, and the third is due to the luminosity.

	y^Z			p_{T}^Z [GeV/c]		$d^2\sigma(Z \to \mu^+\mu^-)/dp_{\mathrm{T}}^Z dy^Z$ [pb]					
2.0	–	2.5	0.0	–	2.2	1.237	±	0.018	±	0.021	±	0.025
2.0	–	2.5	2.2	–	3.4	2.43	±	0.04	±	0.07	±	0.05
2.0	–	2.5	3.4	–	4.6	2.68	±	0.03	±	0.04	±	0.05
2.0	–	2.5	4.6	–	5.8	2.49	±	0.03	±	0.04	±	0.05
2.0	–	2.5	5.8	–	7.2	2.32	±	0.03	±	0.03	±	0.05
2.0	–	2.5	7.2	–	8.7	2.11	±	0.03	±	0.03	±	0.04
2.0	–	2.5	8.7	–	10.5	1.849	±	0.022	±	0.030	±	0.037
2.0	–	2.5	10.5	–	12.8	1.542	±	0.018	±	0.026	±	0.031
2.0	–	2.5	12.8	–	15.4	1.321	±	0.016	±	0.016	±	0.026
2.0	–	2.5	15.4	–	19.0	1.030	±	0.012	±	0.013	±	0.021
2.0	–	2.5	19.0	–	24.5	0.782	±	0.008	±	0.009	±	0.016
2.0	–	2.5	24.5	–	34.0	0.517	±	0.005	±	0.005	±	0.010
2.0	–	2.5	34.0	–	63.0	0.228	±	0.002	±	0.003	±	0.005
2.0	–	2.5	63.0	–	270.0	0.0167	±	0.0002	±	0.0002	±	0.0003
2.5	–	3.0	0.0	–	2.2	3.37	±	0.03	±	0.05	±	0.07
2.5	–	3.0	2.2	–	3.4	6.53	±	0.06	±	0.08	±	0.13
2.5	–	3.0	3.4	–	4.6	6.88	±	0.05	±	0.09	±	0.14
2.5	–	3.0	4.6	–	5.8	6.80	±	0.06	±	0.11	±	0.14
2.5	–	3.0	5.8	–	7.2	6.09	±	0.05	±	0.07	±	0.12
2.5	–	3.0	7.2	–	8.7	5.57	±	0.04	±	0.06	±	0.11
2.5	–	3.0	8.7	–	10.5	4.89	±	0.04	±	0.06	±	0.10
2.5	–	3.0	10.5	–	12.8	4.04	±	0.03	±	0.04	±	0.08
2.5	–	3.0	12.8	–	15.4	3.26	±	0.02	±	0.03	±	0.07
2.5	–	3.0	15.4	–	19.0	2.60	±	0.02	±	0.03	±	0.05
2.5	–	3.0	19.0	–	24.5	1.911	±	0.013	±	0.017	±	0.038
2.5	–	3.0	24.5	–	34.0	1.202	±	0.008	±	0.010	±	0.024
2.5	–	3.0	34.0	–	63.0	0.481	±	0.003	±	0.004	±	0.010
2.5	–	3.0	63.0	–	270.0	0.0289	±	0.0003	±	0.0002	±	0.0006
3.0	–	3.5	0.0	–	2.2	4.16	±	0.04	±	0.06	±	0.08
3.0	–	3.5	2.2	–	3.4	8.06	±	0.06	±	0.10	±	0.16
3.0	–	3.5	3.4	–	4.6	8.25	±	0.06	±	0.13	±	0.17
3.0	–	3.5	4.6	–	5.8	8.17	±	0.06	±	0.10	±	0.16
3.0	–	3.5	5.8	–	7.2	7.25	±	0.05	±	0.07	±	0.14
3.0	–	3.5	7.2	–	8.7	6.26	±	0.05	±	0.10	±	0.13
3.0	–	3.5	8.7	–	10.5	5.56	±	0.04	±	0.06	±	0.11
3.0	–	3.5	10.5	–	12.8	4.51	±	0.03	±	0.04	±	0.09
3.0	–	3.5	12.8	–	15.4	3.63	±	0.03	±	0.03	±	0.07
3.0	–	3.5	15.4	–	19.0	2.81	±	0.02	±	0.02	±	0.06
3.0	–	3.5	19.0	–	24.5	1.966	±	0.013	±	0.033	±	0.039
3.0	–	3.5	24.5	–	34.0	1.175	±	0.008	±	0.010	±	0.024
3.0	–	3.5	34.0	–	63.0	0.429	±	0.003	±	0.005	±	0.009

	y^Z			p_T^Z [GeV/c]		$d^2\sigma(Z \to \mu^+\mu^-)/dp_T^Z dy^Z$ [pb]					
3.0	−	3.5	63.0	−	270.0	0.0202	±	0.0002	±	0.0002	±	0.0004
3.5	−	4.0	0.0	−	2.2	2.25	±	0.03	±	0.04	±	0.04
3.5	−	4.0	2.2	−	3.4	4.44	±	0.05	±	0.09	±	0.09
3.5	−	4.0	3.4	−	4.6	4.37	±	0.05	±	0.09	±	0.09
3.5	−	4.0	4.6	−	5.8	4.25	±	0.05	±	0.06	±	0.08
3.5	−	4.0	5.8	−	7.2	3.60	±	0.04	±	0.06	±	0.07
3.5	−	4.0	7.2	−	8.7	3.29	±	0.03	±	0.05	±	0.07
3.5	−	4.0	8.7	−	10.5	2.78	±	0.03	±	0.06	±	0.06
3.5	−	4.0	10.5	−	12.8	2.37	±	0.02	±	0.03	±	0.05
3.5	−	4.0	12.8	−	15.4	1.849	±	0.019	±	0.026	±	0.037
3.5	−	4.0	15.4	−	19.0	1.407	±	0.014	±	0.025	±	0.028
3.5	−	4.0	19.0	−	24.5	0.952	±	0.009	±	0.011	±	0.019
3.5	−	4.0	24.5	−	34.0	0.576	±	0.006	±	0.008	±	0.012
3.5	−	4.0	34.0	−	63.0	0.188	±	0.002	±	0.003	±	0.004
3.5	−	4.0	63.0	−	270.0	0.00594	±	0.00012	±	0.00021	±	0.00012
4.0	−	4.5	0.0	−	2.2	0.377	±	0.012	±	0.023	±	0.008
4.0	−	4.5	2.2	−	3.4	0.702	±	0.020	±	0.026	±	0.014
4.0	−	4.5	3.4	−	4.6	0.760	±	0.020	±	0.024	±	0.015
4.0	−	4.5	4.6	−	5.8	0.762	±	0.022	±	0.025	±	0.015
4.0	−	4.5	5.8	−	7.2	0.610	±	0.017	±	0.020	±	0.012
4.0	−	4.5	7.2	−	8.7	0.509	±	0.015	±	0.026	±	0.010
4.0	−	4.5	8.7	−	10.5	0.432	±	0.014	±	0.016	±	0.009
4.0	−	4.5	10.5	−	12.8	0.392	±	0.010	±	0.022	±	0.008
4.0	−	4.5	12.8	−	15.4	0.260	±	0.007	±	0.009	±	0.005
4.0	−	4.5	15.4	−	19.0	0.213	±	0.006	±	0.009	±	0.004
4.0	−	4.5	19.0	−	24.5	0.141	±	0.004	±	0.007	±	0.003
4.0	−	4.5	24.5	−	34.0	0.0768	±	0.0021	±	0.0015	±	0.0015
4.0	−	4.5	34.0	−	63.0	0.0211	±	0.0006	±	0.0009	±	0.0004
4.0	−	4.5	63.0	−	270.0	0.00033	±	0.00003	±	0.00001	±	0.00001

Table 17. Measured double differential cross-sections in interval regions of y^Z and p_T^Z. The first uncertainty is statistical, the second systematic, and the third is due to the luminosity.

	y^Z			ϕ_η^*		$d^2\sigma(Z \to \mu^+\mu^-)/d\phi_\eta^* dy^Z$ [pb]					
2.0	−	2.5	0.00	−	0.01	437.3	±	4.7	±	4.3	±	8.7
2.0	−	2.5	0.01	−	0.02	415.4	±	4.5	±	4.8	±	8.3
2.0	−	2.5	0.02	−	0.03	373.3	±	4.3	±	3.0	±	7.5
2.0	−	2.5	0.03	−	0.05	321.4	±	2.8	±	3.1	±	6.4
2.0	−	2.5	0.05	−	0.07	248.0	±	2.5	±	1.9	±	5.0
2.0	−	2.5	0.07	−	0.10	180.9	±	1.7	±	1.4	±	3.6

	y^Z			ϕ^*_η		$d^2\sigma(Z \to \mu^+\mu^-)/d\phi^*_\eta dy^Z$ [pb]						
2.0	−	2.5	0.10	−	0.15	122.6	±	1.1	±	1.3	±	2.5
2.0	−	2.5	0.15	−	0.20	78.78	±	0.87	±	0.83	±	1.58
2.0	−	2.5	0.20	−	0.30	45.68	±	0.47	±	0.56	±	0.91
2.0	−	2.5	0.30	−	0.40	25.61	±	0.35	±	0.26	±	0.51
2.0	−	2.5	0.40	−	0.60	12.57	±	0.17	±	0.16	±	0.25
2.0	−	2.5	0.60	−	0.80	5.68	±	0.11	±	0.08	±	0.11
2.0	−	2.5	0.80	−	1.20	2.34	±	0.05	±	0.03	±	0.05
2.0	−	2.5	1.20	−	2.00	0.554	±	0.018	±	0.010	±	0.011
2.0	−	2.5	2.00	−	4.00	0.0645	±	0.0039	±	0.0015	±	0.0013
2.5	−	3.0	0.00	−	0.01	1145	±	8	±	12	±	23
2.5	−	3.0	0.01	−	0.02	1091	±	7	±	9	±	22
2.5	−	3.0	0.02	−	0.03	984.1	±	7.0	±	10.7	±	19.7
2.5	−	3.0	0.03	−	0.05	815.6	±	4.5	±	5.7	±	16.3
2.5	−	3.0	0.05	−	0.07	631.9	±	3.9	±	4.4	±	12.6
2.5	−	3.0	0.07	−	0.10	459.0	±	2.7	±	3.0	±	9.2
2.5	−	3.0	0.10	−	0.15	297.7	±	1.7	±	2.1	±	6.0
2.5	−	3.0	0.15	−	0.20	187.0	±	1.3	±	1.6	±	3.7
2.5	−	3.0	0.20	−	0.30	107.5	±	0.7	±	0.8	±	2.2
2.5	−	3.0	0.30	−	0.40	55.69	±	0.52	±	0.40	±	1.11
2.5	−	3.0	0.40	−	0.60	26.82	±	0.25	±	0.20	±	0.54
2.5	−	3.0	0.60	−	0.80	11.60	±	0.17	±	0.09	±	0.23
2.5	−	3.0	0.80	−	1.20	4.32	±	0.07	±	0.04	±	0.09
2.5	−	3.0	1.20	−	2.00	1.112	±	0.026	±	0.024	±	0.022
2.5	−	3.0	2.00	−	4.00	0.166	±	0.006	±	0.002	±	0.003
3.0	−	3.5	0.00	−	0.01	1334	±	8	±	10	±	27
3.0	−	3.5	0.01	−	0.02	1264	±	8	±	10	±	25
3.0	−	3.5	0.02	−	0.03	1149	±	8	±	8	±	23
3.0	−	3.5	0.03	−	0.05	934.0	±	4.8	±	6.6	±	18.7
3.0	−	3.5	0.05	−	0.07	708.2	±	4.2	±	5.1	±	14.2
3.0	−	3.5	0.07	−	0.10	509.1	±	2.9	±	4.2	±	10.2
3.0	−	3.5	0.10	−	0.15	319.2	±	1.8	±	2.3	±	6.4
3.0	−	3.5	0.15	−	0.20	194.7	±	1.4	±	1.4	±	3.9
3.0	−	3.5	0.20	−	0.30	107.2	±	0.7	±	1.0	±	2.1
3.0	−	3.5	0.30	−	0.40	53.11	±	0.51	±	0.66	±	1.06
3.0	−	3.5	0.40	−	0.60	24.01	±	0.24	±	0.20	±	0.48
3.0	−	3.5	0.60	−	0.80	9.50	±	0.15	±	0.10	±	0.19

y^Z			ϕ_η^*			$d^2\sigma(Z\to\mu^+\mu^-)/d\phi_\eta^*dy^Z$ [pb]					
3.0	−	3.5	0.80	−	1.20	3.45	±	0.06	±	0.04	±	0.07
3.0	−	3.5	1.20	−	2.00	0.763	±	0.021	±	0.009	±	0.015
3.0	−	3.5	2.00	−	4.00	0.119	±	0.005	±	0.003	±	0.002
3.5	−	4.0	0.00	−	0.01	729.2	±	6.2	±	6.3	±	14.6
3.5	−	4.0	0.01	−	0.02	676.0	±	5.9	±	6.2	±	13.5
3.5	−	4.0	0.02	−	0.03	607.1	±	5.6	±	4.5	±	12.1
3.5	−	4.0	0.03	−	0.05	492.5	±	3.6	±	3.5	±	9.8
3.5	−	4.0	0.05	−	0.07	361.9	±	3.0	±	3.4	±	7.2
3.5	−	4.0	0.07	−	0.10	261.1	±	2.1	±	2.4	±	5.2
3.5	−	4.0	0.10	−	0.15	160.8	±	1.3	±	1.7	±	3.2
3.5	−	4.0	0.15	−	0.20	94.33	±	0.98	±	1.25	±	1.89
3.5	−	4.0	0.20	−	0.30	50.61	±	0.51	±	0.46	±	1.01
3.5	−	4.0	0.30	−	0.40	23.99	±	0.35	±	0.46	±	0.48
3.5	−	4.0	0.40	−	0.60	9.79	±	0.16	±	0.08	±	0.20
3.5	−	4.0	0.60	−	0.80	3.27	±	0.09	±	0.05	±	0.07
3.5	−	4.0	0.80	−	1.20	0.927	±	0.034	±	0.017	±	0.019
3.5	−	4.0	1.20	−	2.00	0.141	±	0.009	±	0.011	±	0.003
3.5	−	4.0	2.00	−	4.00	0.0210	±	0.0023	±	0.0014	±	0.0004
4.0	−	4.5	0.00	−	0.01	121.1	±	2.6	±	2.1	±	2.4
4.0	−	4.5	0.01	−	0.02	112.8	±	2.5	±	2.0	±	2.3
4.0	−	4.5	0.02	−	0.03	98.76	±	2.35	±	1.12	±	1.98
4.0	−	4.5	0.03	−	0.05	80.85	±	1.50	±	1.78	±	1.62
4.0	−	4.5	0.05	−	0.07	58.34	±	1.27	±	0.59	±	1.17
4.0	−	4.5	0.07	−	0.10	39.44	±	0.85	±	0.62	±	0.79
4.0	−	4.5	0.10	−	0.15	25.03	±	0.52	±	0.50	±	0.50
4.0	−	4.5	0.15	−	0.20	13.26	±	0.38	±	0.28	±	0.27
4.0	−	4.5	0.20	−	0.30	6.62	±	0.19	±	0.09	±	0.13
4.0	−	4.5	0.30	−	0.40	2.85	±	0.13	±	0.19	±	0.06
4.0	−	4.5	0.40	−	0.60	0.992	±	0.052	±	0.018	±	0.020
4.0	−	4.5	0.60	−	0.80	0.238	±	0.025	±	0.013	±	0.005
4.0	−	4.5	0.80	−	1.20	0.0248	±	0.0060	±	0.0026	±	0.0005
4.0	−	4.5	1.20	−	2.00	0.00241	±	0.00140	±	0.00092	±	0.00005
4.0	−	4.5	2.00	−	4.00	0.00060	±	0.00060	±	0.00055	±	0.00001

Table 18. Measured double differential cross-sections in interval regions of y^Z and ϕ_η^*. The first uncertainty is statistical, the second systematic, and the third is due to the luminosity.

y^Z			Eff	BKG	FSR	Closure	Alignment
2.000	–	2.125	0.70	0.36	0.12	0.91	0.27
2.125	–	2.250	0.68	0.28	0.20	0.71	0.22
2.250	–	2.375	0.66	0.28	0.03	0.58	0.14
2.375	–	2.500	0.65	0.27	0.08	0.21	0.07
2.500	–	2.625	0.65	0.22	0.10	0.14	0.06
2.625	–	2.750	0.65	0.19	0.01	0.19	0.08
2.750	–	2.875	0.65	0.18	0.15	0.06	0.13
2.875	–	3.000	0.64	0.14	0.03	0.01	0.10
3.000	–	3.125	0.64	0.15	0.03	0.01	0.06
3.125	–	3.250	0.65	0.11	0.04	0.06	0.07
3.250	–	3.375	0.65	0.11	0.08	0.39	0.10
3.375	–	3.500	0.65	0.07	0.16	0.30	0.09
3.500	–	3.625	0.65	0.07	0.05	0.29	0.10
3.625	–	3.750	0.66	0.10	0.18	0.75	0.17
3.750	–	3.875	0.67	0.09	0.33	0.27	0.13
3.875	–	4.000	0.68	0.09	0.04	0.75	0.13
4.000	–	4.250	0.70	0.09	0.14	0.81	0.07
4.250	–	4.500	0.78	0.25	0.28	2.85	0.49

Table 19. Systematic uncertainties in the single differential cross-sections in interval regions of y^Z, presented in percentage. The contributions from efficiency (Eff), background (BKG), final state radiation (FSR), closure test (Closure), and alignment and calibration (Alignment) are shown.

p_T^Z [GeV/c]			Eff	BKG	FSR	Closure	Alignment	Unfold
0.0	–	2.2	0.81	0.05	0.24	0.50	1.10	0.21
2.2	–	3.4	0.83	0.08	0.67	0.18	0.82	0.33
3.4	–	4.6	0.77	0.07	0.51	0.45	0.77	0.51
4.6	–	5.8	0.80	0.08	0.18	0.31	0.86	0.46
5.8	–	7.2	0.78	0.07	0.24	0.44	0.61	0.20
7.2	–	8.7	0.78	0.10	0.66	0.33	0.73	0.27
8.7	–	10.5	0.79	0.09	0.51	0.24	0.59	0.32
10.5	–	12.8	0.77	0.10	0.43	0.34	0.39	0.30
12.8	–	15.4	0.77	0.11	0.36	0.22	0.43	0.20
15.4	–	19.0	0.77	0.12	0.52	0.43	0.36	0.09
19.0	–	24.5	0.77	0.11	0.62	0.46	0.32	0.15
24.5	–	34.0	0.77	0.08	0.14	0.42	0.24	0.10
34.0	–	63.0	0.76	0.07	0.13	0.72	0.14	0.03
63.0	–	270.0	0.77	0.11	0.37	0.54	0.27	0.06

Table 20. Systematic uncertainties in the single differential cross-sections in interval regions of p_T^Z, presented in percentage. The contributions from efficiency (Eff), background (BKG), final state radiation (FSR), closure test (Closure), unfolding (Unfold), and alignment and calibration (Alignment) are shown.

ϕ_η^*			Eff	BKG	FSR	Closure	Alignment
0.00	−	0.01	0.77	0.06	0.20	0.43	0.04
0.01	−	0.02	0.77	0.06	0.30	0.32	0.06
0.02	−	0.03	0.77	0.07	0.17	0.32	0.06
0.03	−	0.05	0.77	0.07	0.14	0.17	0.07
0.05	−	0.07	0.77	0.07	0.19	0.14	0.07
0.07	−	0.10	0.77	0.08	0.22	0.21	0.06
0.10	−	0.15	0.77	0.07	0.07	0.38	0.04
0.15	−	0.20	0.77	0.08	0.26	0.36	0.10
0.20	−	0.30	0.77	0.06	0.28	0.40	0.06
0.30	−	0.40	0.77	0.10	0.17	0.68	0.08
0.40	−	0.60	0.77	0.10	0.24	0.25	0.11
0.60	−	0.80	0.78	0.17	0.34	0.44	0.14
0.80	−	1.20	0.78	0.15	0.26	0.60	0.19
1.20	−	2.00	0.80	0.33	1.18	0.66	0.19
2.00	−	4.00	0.82	0.40	1.02	0.91	0.38

Table 21. Systematic uncertainties in the single differential cross-sections in interval regions of ϕ_η^*, presented in percentage. The contributions from efficiency (Eff), background (BKG), final state radiation (FSR), closure test (Closure), and alignment and calibration (Alignment) are shown.

y^Z			p_T^Z [GeV/c]			Eff	BKG	FSR	Closure	Alignment	Unfold
2.0	−	2.5	0.0	−	2.2	0.73	0.22	0.65	0.85	1.04	0.20
2.0	−	2.5	2.2	−	3.4	0.73	0.18	2.11	0.48	1.38	0.40
2.0	−	2.5	3.4	−	4.6	0.69	0.17	0.80	0.61	0.66	0.41
2.0	−	2.5	4.6	−	5.8	0.74	0.22	0.04	0.06	1.18	0.47
2.0	−	2.5	5.8	−	7.2	0.68	0.19	0.39	0.36	0.88	0.24
2.0	−	2.5	7.2	−	8.7	0.68	0.19	0.31	0.54	0.77	0.29
2.0	−	2.5	8.7	−	10.5	0.67	0.41	0.35	1.18	0.65	0.12
2.0	−	2.5	10.5	−	12.8	0.68	0.17	1.36	0.32	0.62	0.33
2.0	−	2.5	12.8	−	15.4	0.67	0.27	0.71	0.33	0.51	0.30
2.0	−	2.5	15.4	−	19.0	0.69	0.19	0.47	0.80	0.48	0.18
2.0	−	2.5	19.0	−	24.5	0.67	0.16	0.26	0.85	0.33	0.09
2.0	−	2.5	24.5	−	34.0	0.67	0.24	0.14	0.55	0.33	0.08
2.0	−	2.5	34.0	−	63.0	0.67	0.15	0.28	0.87	0.38	0.02
2.0	−	2.5	63.0	−	270.0	0.67	0.25	0.65	1.09	0.24	0.09
2.5	−	3.0	0.0	−	2.2	0.71	0.04	0.11	0.62	1.02	0.17
2.5	−	3.0	2.2	−	3.4	0.78	0.08	0.59	0.04	0.66	0.41
2.5	−	3.0	3.4	−	4.6	0.66	0.13	0.22	0.36	0.87	0.63
2.5	−	3.0	4.6	−	5.8	0.68	0.13	0.34	0.88	0.99	0.46
2.5	−	3.0	5.8	−	7.2	0.67	0.13	0.05	0.29	0.92	0.28
2.5	−	3.0	7.2	−	8.7	0.66	0.16	0.30	0.62	0.44	0.32

	y^Z			p_T^Z [GeV/c]		Eff	BKG	FSR	Closure	Alignment	Unfold
2.5	−	3.0	8.7	−	10.5	0.66	0.14	0.91	0.03	0.43	0.16
2.5	−	3.0	10.5	−	12.8	0.66	0.22	0.10	0.44	0.43	0.18
2.5	−	3.0	12.8	−	15.4	0.66	0.21	0.27	0.20	0.58	0.24
2.5	−	3.0	15.4	−	19.0	0.65	0.24	0.87	0.42	0.41	0.04
2.5	−	3.0	19.0	−	24.5	0.65	0.18	0.53	0.07	0.29	0.05
2.5	−	3.0	24.5	−	34.0	0.65	0.08	0.13	0.36	0.30	0.07
2.5	−	3.0	34.0	−	63.0	0.65	0.11	0.16	0.59	0.10	0.04
2.5	−	3.0	63.0	−	270.0	0.65	0.15	0.09	0.14	0.32	0.02
3.0	−	3.5	0.0	−	2.2	0.72	0.09	0.22	0.29	1.14	0.12
3.0	−	3.5	2.2	−	3.4	0.66	0.14	0.54	0.07	0.76	0.33
3.0	−	3.5	3.4	−	4.6	0.66	0.15	0.92	0.77	0.60	0.57
3.0	−	3.5	4.6	−	5.8	0.68	0.19	0.19	0.03	0.84	0.48
3.0	−	3.5	5.8	−	7.2	0.67	0.10	0.19	0.47	0.48	0.08
3.0	−	3.5	7.2	−	8.7	0.73	0.17	1.16	0.13	0.69	0.30
3.0	−	3.5	8.7	−	10.5	0.66	0.16	0.32	0.23	0.40	0.56
3.0	−	3.5	10.5	−	12.8	0.65	0.16	0.48	0.12	0.21	0.36
3.0	−	3.5	12.8	−	15.4	0.66	0.19	0.30	0.10	0.38	0.09
3.0	−	3.5	15.4	−	19.0	0.65	0.23	0.24	0.13	0.24	0.07
3.0	−	3.5	19.0	−	24.5	0.65	0.20	1.23	0.84	0.36	0.12
3.0	−	3.5	24.5	−	34.0	0.65	0.16	0.17	0.44	0.15	0.17
3.0	−	3.5	34.0	−	63.0	0.65	0.12	0.09	1.05	0.15	0.02
3.0	−	3.5	63.0	−	270.0	0.65	0.20	0.73	0.26	0.33	0.13
3.5	−	4.0	0.0	−	2.2	0.80	0.05	0.37	0.37	1.55	0.29
3.5	−	4.0	2.2	−	3.4	0.73	0.20	1.12	0.33	1.31	0.50
3.5	−	4.0	3.4	−	4.6	0.69	0.09	0.43	0.39	1.58	0.83
3.5	−	4.0	4.6	−	5.8	0.73	0.09	0.12	0.08	1.07	0.67
3.5	−	4.0	5.8	−	7.2	0.68	0.10	0.78	0.98	0.69	0.38
3.5	−	4.0	7.2	−	8.7	0.67	0.29	0.86	0.25	1.07	0.54
3.5	−	4.0	8.7	−	10.5	0.70	0.10	0.94	0.01	1.67	0.47
3.5	−	4.0	10.5	−	12.8	0.71	0.09	0.86	0.53	0.44	0.54
3.5	−	4.0	12.8	−	15.4	0.66	0.23	0.88	0.62	0.49	0.40
3.5	−	4.0	15.4	−	19.0	0.67	0.15	0.72	1.37	0.55	0.23
3.5	−	4.0	19.0	−	24.5	0.68	0.15	0.31	0.30	0.67	0.55
3.5	−	4.0	24.5	−	34.0	0.66	0.11	0.27	1.00	0.54	0.12
3.5	−	4.0	34.0	−	63.0	0.66	0.15	0.17	1.13	0.11	0.11
3.5	−	4.0	63.0	−	270.0	0.66	0.30	0.73	3.36	0.67	0.24
4.0	−	4.5	0.0	−	2.2	0.75	0.13	1.43	5.50	1.71	0.71
4.0	−	4.5	2.2	−	3.4	0.72	0.47	0.92	2.30	2.35	1.21
4.0	−	4.5	3.4	−	4.6	0.73	0.50	1.24	0.67	2.57	0.49
4.0	−	4.5	4.6	−	5.8	0.81	0.43	0.71	1.29	2.36	1.33
4.0	−	4.5	5.8	−	7.2	0.79	0.39	0.63	2.54	1.38	1.32

	y^{Z}			p_{T}^{Z} [GeV/c]		Eff	BKG	FSR	Closure	Alignment	Unfold
4.0	−	4.5	7.2	−	8.7	0.85	0.20	3.74	1.99	1.86	1.78
4.0	−	4.5	8.7	−	10.5	0.83	0.15	0.42	2.19	2.39	1.33
4.0	−	4.5	10.5	−	12.8	0.72	0.47	0.36	3.73	3.65	2.06
4.0	−	4.5	12.8	−	15.4	0.74	0.15	0.96	1.08	2.21	1.91
4.0	−	4.5	15.4	−	19.0	0.74	0.22	3.72	0.07	2.06	0.98
4.0	−	4.5	19.0	−	24.5	0.77	0.68	2.58	3.51	1.29	0.44
4.0	−	4.5	24.5	−	34.0	0.71	0.24	0.94	0.69	0.96	1.01
4.0	−	4.5	34.0	−	63.0	0.71	0.21	0.57	4.16	0.63	0.32
4.0	−	4.5	63.0	−	270.0	0.69	0.45	1.40	0.93	2.68	1.06

Table 22. Systematic uncertainties in the double differential cross-sections in interval regions of y^{Z} and p_{T}^{Z}, presented in percentage. The contributions from efficiency (Eff), background (BKG), final state radiation (FSR), closure test (Closure), unfolding (Unfold), and alignment and calibration (Alignment) are shown.

	y^{Z}			ϕ_η^*		Eff	BKG	FSR	Closure	Alignment
2.0	−	2.5	0.00	−	0.01	0.67	0.15	0.03	0.72	0.06
2.0	−	2.5	0.01	−	0.02	0.67	0.19	0.50	0.77	0.15
2.0	−	2.5	0.02	−	0.03	0.67	0.22	0.38	0.10	0.08
2.0	−	2.5	0.03	−	0.05	0.67	0.18	0.22	0.61	0.06
2.0	−	2.5	0.05	−	0.07	0.67	0.13	0.33	0.13	0.08
2.0	−	2.5	0.07	−	0.10	0.67	0.14	0.26	0.15	0.11
2.0	−	2.5	0.10	−	0.15	0.67	0.21	0.01	0.82	0.05
2.0	−	2.5	0.15	−	0.20	0.67	0.17	0.45	0.67	0.06
2.0	−	2.5	0.20	−	0.30	0.67	0.18	0.34	0.96	0.05
2.0	−	2.5	0.30	−	0.40	0.67	0.28	0.35	0.60	0.10
2.0	−	2.5	0.40	−	0.60	0.67	0.25	0.19	1.00	0.12
2.0	−	2.5	0.60	−	0.80	0.67	0.31	0.86	0.76	0.30
2.0	−	2.5	0.80	−	1.20	0.67	0.36	0.22	1.05	0.26
2.0	−	2.5	1.20	−	2.00	0.67	0.69	1.42	0.72	0.18
2.0	−	2.5	2.00	−	4.00	0.67	0.66	0.50	1.92	0.78
2.5	−	3.0	0.00	−	0.01	0.65	0.13	0.38	0.70	0.05
2.5	−	3.0	0.01	−	0.02	0.65	0.13	0.50	0.25	0.07
2.5	−	3.0	0.02	−	0.03	0.65	0.16	0.33	0.78	0.09
2.5	−	3.0	0.03	−	0.05	0.65	0.09	0.22	0.00	0.07
2.5	−	3.0	0.05	−	0.07	0.65	0.13	0.17	0.02	0.10
2.5	−	3.0	0.07	−	0.10	0.65	0.11	0.08	0.05	0.04
2.5	−	3.0	0.10	−	0.15	0.65	0.11	0.05	0.27	0.05
2.5	−	3.0	0.15	−	0.20	0.65	0.15	0.36	0.39	0.07
2.5	−	3.0	0.20	−	0.30	0.65	0.08	0.09	0.40	0.11
2.5	−	3.0	0.30	−	0.40	0.65	0.16	0.23	0.08	0.10

	y^Z			ϕ_η^*		Eff	BKG	FSR	Closure	Alignment
2.5	−	3.0	0.40	−	0.60	0.65	0.10	0.31	0.01	0.13
2.5	−	3.0	0.60	−	0.80	0.65	0.25	0.02	0.31	0.13
2.5	−	3.0	0.80	−	1.20	0.65	0.28	0.47	0.19	0.23
2.5	−	3.0	1.20	−	2.00	0.65	0.34	1.98	0.27	0.18
2.5	−	3.0	2.00	−	4.00	0.66	0.28	0.35	0.60	0.27
3.0	−	3.5	0.00	−	0.01	0.65	0.09	0.11	0.39	0.03
3.0	−	3.5	0.01	−	0.02	0.65	0.08	0.14	0.36	0.06
3.0	−	3.5	0.02	−	0.03	0.65	0.11	0.11	0.15	0.05
3.0	−	3.5	0.03	−	0.05	0.65	0.16	0.15	0.14	0.06
3.0	−	3.5	0.05	−	0.07	0.66	0.11	0.25	0.08	0.06
3.0	−	3.5	0.07	−	0.10	0.65	0.17	0.35	0.32	0.07
3.0	−	3.5	0.10	−	0.15	0.65	0.14	0.01	0.31	0.04
3.0	−	3.5	0.15	−	0.20	0.65	0.13	0.22	0.05	0.15
3.0	−	3.5	0.20	−	0.30	0.65	0.09	0.48	0.50	0.03
3.0	−	3.5	0.30	−	0.40	0.65	0.18	0.12	1.03	0.09
3.0	−	3.5	0.40	−	0.60	0.65	0.25	0.38	0.26	0.12
3.0	−	3.5	0.60	−	0.80	0.66	0.30	0.53	0.58	0.08
3.0	−	3.5	0.80	−	1.20	0.65	0.20	0.09	0.96	0.16
3.0	−	3.5	1.20	−	2.00	0.66	0.77	0.37	0.45	0.31
3.0	−	3.5	2.00	−	4.00	0.66	0.40	2.56	0.67	0.35
3.5	−	4.0	0.00	−	0.01	0.67	0.11	0.43	0.32	0.09
3.5	−	4.0	0.01	−	0.02	0.67	0.09	0.37	0.51	0.06
3.5	−	4.0	0.02	−	0.03	0.67	0.13	0.12	0.24	0.10
3.5	−	4.0	0.03	−	0.05	0.66	0.09	0.10	0.10	0.15
3.5	−	4.0	0.05	−	0.07	0.67	0.14	0.22	0.62	0.10
3.5	−	4.0	0.07	−	0.10	0.67	0.08	0.39	0.46	0.13
3.5	−	4.0	0.10	−	0.15	0.66	0.10	0.29	0.78	0.07
3.5	−	4.0	0.15	−	0.20	0.66	0.14	0.19	1.10	0.25
3.5	−	4.0	0.20	−	0.30	0.66	0.14	0.52	0.28	0.07
3.5	−	4.0	0.30	−	0.40	0.67	0.15	0.13	1.77	0.11
3.5	−	4.0	0.40	−	0.60	0.66	0.25	0.17	0.16	0.33
3.5	−	4.0	0.60	−	0.80	0.66	0.74	0.69	0.71	0.34
3.5	−	4.0	0.80	−	1.20	0.66	0.14	0.28	1.55	0.58
3.5	−	4.0	1.20	−	2.00	0.68	0.42	1.95	7.26	0.71
3.5	−	4.0	2.00	−	4.00	0.68	0.50	1.78	5.58	2.56
4.0	−	4.5	0.00	−	0.01	0.71	0.26	0.21	1.50	0.30
4.0	−	4.5	0.01	−	0.02	0.71	0.05	1.57	0.31	0.16
4.0	−	4.5	0.02	−	0.03	0.71	0.40	0.20	0.74	0.19
4.0	−	4.5	0.03	−	0.05	0.71	0.25	0.38	2.03	0.10
4.0	−	4.5	0.05	−	0.07	0.71	0.35	0.57	0.09	0.21
4.0	−	4.5	0.07	−	0.10	0.71	0.27	0.68	1.20	0.18

	y^{Z}			ϕ_η^*		Eff	BKG	FSR	Closure	Alignment
4.0	−	4.5	0.10	−	0.15	0.71	0.04	0.44	1.79	0.35
4.0	−	4.5	0.15	−	0.20	0.71	0.18	1.64	0.98	0.36
4.0	−	4.5	0.20	−	0.30	0.71	0.03	0.86	0.49	0.41
4.0	−	4.5	0.30	−	0.40	0.75	0.38	1.09	6.43	0.65
4.0	−	4.5	0.40	−	0.60	0.70	0.08	0.81	1.10	0.97
4.0	−	4.5	0.60	−	0.80	0.70	0.25	0.07	5.31	1.62
4.0	−	4.5	0.80	−	1.20	0.71	0.00	7.46	6.39	3.97
4.0	−	4.5	1.20	−	2.00	12.06	18.37	24.14	0.23	19.98
4.0	−	4.5	2.00	−	4.00	38.09	61.98	4.01	20.47	51.95

Table 23. Systematic uncertainties in the double differential cross-sections in interval regions of y^{Z} and ϕ_η^*, presented in percentage. The contributions from efficiency (Eff), background (BKG), final state radiation (FSR), closure test (Closure), and alignment and calibration (Alignment) are shown.

References

[1] S. Camarda, L. Cieri and G. Ferrera, *Drell-Yan lepton-pair production: qT resummation at N^3LL accuracy and fiducial cross sections at N^3LO*, *Phys. Rev. D* **104** (2021) L111503 [`arXiv:2103.04974`] [InSPIRE].

[2] C. Duhr and B. Mistlberger, *Lepton-pair production at hadron colliders at N^3LO in QCD*, *JHEP* **03** (2022) 116 [`arXiv:2111.10379`] [InSPIRE].

[3] P.J. Rijken and W.L. van Neerven, *Order α_s^2 contributions to the Drell-Yan cross-section at fixed target energies*, *Phys. Rev. D* **51** (1995) 44 [`hep-ph/9408366`] [InSPIRE].

[4] R. Hamberg, W.L. van Neerven and T. Matsuura, *A complete calculation of the order α_s^2 correction to the Drell-Yan K factor*, *Nucl. Phys. B* **359** (1991) 343 [*Erratum ibid.* **644** (2002) 403] [InSPIRE].

[5] R.V. Harlander and W.B. Kilgore, *Next-to-next-to-leading order Higgs production at hadron colliders*, *Phys. Rev. Lett.* **88** (2002) 201801 [`hep-ph/0201206`] [InSPIRE].

[6] W.L. van Neerven and E.B. Zijlstra, *The $O(\alpha_s^2)$ corrected Drell-Yan K factor in the DIS and MS scheme*, *Nucl. Phys. B* **382** (1992) 11 [*Erratum ibid.* **680** (2004) 513] [InSPIRE].

[7] C. Anastasiou, L.J. Dixon, K. Melnikov and F. Petriello, *High precision QCD at hadron colliders: Electroweak gauge boson rapidity distributions at NNLO*, *Phys. Rev. D* **69** (2004) 094008 [`hep-ph/0312266`] [InSPIRE].

[8] I. Scimemi and A. Vladimirov, *Non-perturbative structure of semi-inclusive deep-inelastic and Drell-Yan scattering at small transverse momentum*, *JHEP* **06** (2020) 137 [`arXiv:1912.06532`] [InSPIRE].

[9] M. Bury, F. Hautmann, S. Leal-Gomez, I. Scimemi, A. Vladimirov and P. Zurita, *PDF bias and flavor dependence in TMD distributions*, arXiv:2201.07114 [INSPIRE].

[10] LHCb collaboration, *Measurement of the W boson mass*, *JHEP* **01** (2022) 036 [arXiv:2109.01113] [INSPIRE].

[11] LHCb collaboration, *Measurement of the forward-backward asymmetry in $Z/\gamma^* \to \mu^+\mu^-$ decays and determination of the effective weak mixing angle*, *JHEP* **11** (2015) 190 [arXiv:1509.07645] [INSPIRE].

[12] H1 and ZEUS collaborations, *Combined Measurement and QCD Analysis of the Inclusive $e^\pm p$ Scattering Cross Sections at HERA*, *JHEP* **01** (2010) 109 [arXiv:0911.0884] [INSPIRE].

[13] H1 and ZEUS collaborations, *Combination of measurements of inclusive deep inelastic $e^\pm p$ scattering cross sections and QCD analysis of HERA data*, *Eur. Phys. J. C* **75** (2015) 580 [arXiv:1506.06042] [INSPIRE].

[14] CDF collaboration, *Forward-backward charge asymmetry of electron pairs above the Z^0 pole*, *Phys. Rev. Lett.* **77** (1996) 2616 [INSPIRE].

[15] CDF collaboration, *Measurement of the forward-backward charge asymmetry from $W \to e\nu$ production in $p\bar{p}$ collisions at $\sqrt{s} = 1.96$ TeV*, *Phys. Rev. D* **71** (2005) 051104 [hep-ex/0501023] [INSPIRE].

[16] CDF collaboration, *Measurement of $d\sigma/dy$ of Drell-Yan e^+e^- pairs in the Z Mass Region from $p\bar{p}$ Collisions at $\sqrt{s} = 1.96$ TeV*, *Phys. Lett. B* **692** (2010) 232 [arXiv:0908.3914] [INSPIRE].

[17] CDF collaboration, *Measurement of the Inclusive Jet Cross Section at the Fermilab Tevatron $p\bar{p}$ Collider Using a Cone-Based Jet Algorithm*, *Phys. Rev. D* **78** (2008) 052006 [*Erratum ibid.* **79** (2009) 119902] [arXiv:0807.2204] [INSPIRE].

[18] D0 collaboration, *Measurement of the muon charge asymmetry from W boson decays*, *Phys. Rev. D* **77** (2008) 011106 [arXiv:0709.4254] [INSPIRE].

[19] D0 collaboration, *Measurement of the ratios of the $Z/\gamma^* + \geq n$ jet production cross sections to the total inclusive Z/γ^* cross section in $p\bar{p}$ collisions at $\sqrt{s} = 1.96$ TeV*, *Phys. Lett. B* **658** (2008) 112 [hep-ex/0608052] [INSPIRE].

[20] D0 collaboration, *Measurement of the electron charge asymmetry in $p\bar{p} \to W + X \to e\nu + X$ decays in $p\bar{p}$ collisions at $\sqrt{s} = 1.96$ TeV*, *Phys. Rev. D* **91** (2015) 032007 [*Erratum ibid.* **91** (2015) 079901] [arXiv:1412.2862] [INSPIRE].

[21] D0 collaboration, *Measurement of the inclusive jet cross-section in $p\bar{p}$ collisions at $\sqrt{s} = 1.96$ TeV*, *Phys. Rev. Lett.* **101** (2008) 062001 [arXiv:0802.2400] [INSPIRE].

[22] ATLAS collaboration, *Measurement of the inclusive $W^\pm$ and Z/γ^* cross sections in the electron and muon decay channels in pp collisions at $\sqrt{s} = 7$ TeV with the ATLAS detector*, *Phys. Rev. D* **85** (2012) 072004 [arXiv:1109.5141] [INSPIRE].

[23] ATLAS collaboration, *Measurement of the transverse momentum and ϕ_η^* distributions of Drell-Yan lepton pairs in proton-proton collisions at $\sqrt{s} = 8$ TeV with the ATLAS detector*, *Eur. Phys. J. C* **76** (2016) 291 [arXiv:1512.02192] [INSPIRE].

[24] CMS collaboration, *Measurement of the Muon Charge Asymmetry in Inclusive $pp \to W + X$ Production at $\sqrt{s} = 7$ TeV and an Improved Determination of Light Parton Distribution Functions*, *Phys. Rev. D* **90** (2014) 032004 [arXiv:1312.6283] [INSPIRE].

[25] CMS collaboration, *Measurement of the Electron Charge Asymmetry in Inclusive W Production in pp Collisions at $\sqrt{s} = 7$ TeV*, *Phys. Rev. Lett.* **109** (2012) 111806 [arXiv:1206.2598] [INSPIRE].

[26] ATLAS collaboration, *Measurement of the transverse momentum distribution of Drell-Yan lepton pairs in proton-proton collisions at $\sqrt{s} = 13$ TeV with the ATLAS detector*, *Eur. Phys. J. C* **80** (2020) 616 [arXiv:1912.02844] [INSPIRE].

[27] CMS collaboration, *Measurements of differential Z boson production cross sections in proton-proton collisions at $\sqrt{s} = 13$ TeV*, *JHEP* **12** (2019) 061 [arXiv:1909.04133] [INSPIRE].

[28] LHCb collaboration, *Measurement of the forward W boson cross-section in pp collisions at $\sqrt{s} = 7$ TeV*, *JHEP* **12** (2014) 079 [arXiv:1408.4354] [INSPIRE].

[29] LHCb collaboration, *Measurement of the forward Z boson production cross-section in pp collisions at $\sqrt{s} = 7$ TeV*, *JHEP* **08** (2015) 039 [arXiv:1505.07024] [INSPIRE].

[30] LHCb collaboration, *Measurement of forward $Z \to e^+e^-$ production at $\sqrt{s} = 8$ TeV*, *JHEP* **05** (2015) 109 [arXiv:1503.00963] [INSPIRE].

[31] LHCb collaboration, *Measurement of forward W and Z boson production in pp collisions at $\sqrt{s} = 8$ TeV*, *JHEP* **01** (2016) 155 [arXiv:1511.08039] [INSPIRE].

[32] LHCb collaboration, *Measurement of forward $W \to e\nu$ production in pp collisions at $\sqrt{s} = 8$ TeV*, *JHEP* **10** (2016) 030 [arXiv:1608.01484] [INSPIRE].

[33] LHCb collaboration, *Measurement of the forward Z boson production cross-section in pp collisions at $\sqrt{s} = 13$ TeV*, *JHEP* **09** (2016) 136 [arXiv:1607.06495] [INSPIRE].

[34] S. Dulat et al., *New parton distribution functions from a global analysis of quantum chromodynamics*, *Phys. Rev. D* **93** (2016) 033006 [arXiv:1506.07443] [INSPIRE].

[35] L.A. Harland-Lang, A.D. Martin, P. Motylinski and R.S. Thorne, *Parton distributions in the LHC era: MMHT 2014 PDFs*, *Eur. Phys. J. C* **75** (2015) 204 [arXiv:1412.3989] [INSPIRE].

[36] NNPDF collaboration, *Parton distributions for the LHC Run II*, *JHEP* **04** (2015) 040 [arXiv:1410.8849] [INSPIRE].

[37] T.-J. Hou et al., *New CTEQ global analysis of quantum chromodynamics with high-precision data from the LHC*, *Phys. Rev. D* **103** (2021) 014013 [arXiv:1912.10053] [INSPIRE].

[38] NNPDF collaboration, *Improving quark flavor separation with forward W and Z production at LHCb*, *PoS* **DIS2017** (2018) 198 [arXiv:1705.04468] [INSPIRE].

[39] Q. Deng, Q. Han, H. Yin, S. Dulat, T.-J. Hou and C.P. Yuan, *Impact of LHCb 13 TeV W and Z pseudo-data on the Parton Distribution Functions*, *Chin. Phys. C* **45** (2021) 023110 [arXiv:2009.03181] [INSPIRE].

[40] SEAQUEST collaboration, *The asymmetry of antimatter in the proton*, *Nature* **590** (2021) 561 [*Erratum ibid.* **604** (2022) E26] [arXiv:2103.04024] [INSPIRE].

[41] NUSEA collaboration, *Improved measurement of the $\bar{d}/\bar{u}$ asymmetry in the nucleon sea*, *Phys. Rev. D* **64** (2001) 052002 [hep-ex/0103030] [INSPIRE].

[42] LHCb collaboration, *Precision luminosity measurements at LHCb*, 2014 *JINST* **9** P12005 [arXiv:1410.0149] [INSPIRE].

[43] D0 collaboration, *Precise Study of the Z/γ^* Boson Transverse Momentum Distribution in $p\bar{p}$ Collisions using a Novel Technique*, *Phys. Rev. Lett.* **106** (2011) 122001 [`arXiv:1010.0262`] [InSPIRE].

[44] LHCb collaboration, *The LHCb Detector at the LHC*, 2008 *JINST* **3** S08005 [InSPIRE].

[45] LHCb collaboration, *LHCb Detector Performance*, *Int. J. Mod. Phys. A* **30** (2015) 1530022 [`arXiv:1412.6352`] [InSPIRE].

[46] R. Aaij et al., *Performance of the LHCb Vertex Locator*, 2014 *JINST* **9** P09007 [`arXiv:1405.7808`] [InSPIRE].

[47] LHCb collaboration, *LHCb reoptimized detector design and performance: Technical Design Report*, CERN-LHCC-2003-030 (2003).

[48] P. d'Argent et al., *Improved performance of the LHCb Outer Tracker in LHC Run 2*, 2017 *JINST* **12** P11016 [`arXiv:1708.00819`] [InSPIRE].

[49] A.A. Alves Jr. et al., *Performance of the LHCb muon system*, 2013 *JINST* **8** P02022 [`arXiv:1211.1346`] [InSPIRE].

[50] R. Aaij et al., *The LHCb Trigger and its Performance in 2011*, 2013 *JINST* **8** P04022 [`arXiv:1211.3055`] [InSPIRE].

[51] T. Sjöstrand, S. Mrenna and P.Z. Skands, *PYTHIA 6.4 Physics and Manual*, *JHEP* **05** (2006) 026 [`hep-ph/0603175`] [InSPIRE].

[52] I. Belyaev et al., *Handling of the generation of primary events in Gauss, the LHCb simulation framework*, *J. Phys. Conf. Ser.* **331** (2011) 032047 [InSPIRE].

[53] N. Davidson, T. Przedzinski and Z. Was, *PHOTOS interface in C++: Technical and Physics Documentation*, *Comput. Phys. Commun.* **199** (2016) 86 [`arXiv:1011.0937`] [InSPIRE].

[54] J. Allison et al., *Geant4 developments and applications*, *IEEE Trans. Nucl. Sci.* **53** (2006) 270 [InSPIRE].

[55] M. Clemencic et al., *The LHCb simulation application, Gauss: Design, evolution and experience*, *J. Phys. Conf. Ser.* **331** (2011) 032023 [InSPIRE].

[56] R. Gavin, Y. Li, F. Petriello and S. Quackenbush, *FEWZ 2.0: A code for hadronic Z production at next-to-next-to-leading order*, *Comput. Phys. Commun.* **182** (2011) 2388 [`arXiv:1011.3540`] [InSPIRE].

[57] LHCb collaboration, *Measurement of forward top pair production in the dilepton channel in pp collisions at $\sqrt{s} = 13$ TeV*, *JHEP* **08** (2018) 174 [`arXiv:1803.05188`] [InSPIRE].

[58] R. Aaij et al., *Design and performance of the LHCb trigger and full real-time reconstruction in Run 2 of the LHC*, 2019 *JINST* **14** P04013 [`arXiv:1812.10790`] [InSPIRE].

[59] Particle Data collaboration, *Review of Particle Physics*, *Prog. Theor. Exp. Phys.* **2020** (2020) 083C01 [InSPIRE].

[60] LHCb collaboration, *Measurement of the track reconstruction efficiency at LHCb*, 2015 *JINST* **10** P02007 [`arXiv:1408.1251`] [InSPIRE].

[61] G. D'Agostini, *A Multidimensional unfolding method based on Bayes' theorem*, *Nucl. Instrum. Meth. A* **362** (1995) 487 [InSPIRE].

[62] C. Balázs and C.P. Yuan, *Soft gluon effects on lepton pairs at hadron colliders*, *Phys. Rev. D* **56** (1997) 5558 [`hep-ph/9704258`] [InSPIRE].

[63] T. Adye, *Unfolding algorithms and tests using RooUnfold*, arXiv:1105.1160 [InSPIRE].

[64] L. Lyons, D. Gibaut and P. Clifford, *How to Combine Correlated Estimates of a Single Physical Quantity*, *Nucl. Instrum. Meth. A* **270** (1988) 110 [InSPIRE].

[65] A. Valassi, *Combining correlated measurements of several different physical quantities*, *Nucl. Instrum. Meth. A* **500** (2003) 391 [InSPIRE].

[66] J.C. Collins, D.E. Soper and G.F. Sterman, *Transverse Momentum Distribution in Drell-Yan Pair and W and Z Boson Production*, *Nucl. Phys. B* **250** (1985) 199 [InSPIRE].

[67] J.C. Collins and D.E. Soper, *Back-To-Back Jets in QCD*, *Nucl. Phys. B* **193** (1981) 381 [*Erratum ibid.* **213** (1983) 545] [InSPIRE].

[68] J.C. Collins and D.E. Soper, *Back-To-Back Jets: Fourier Transform from B to K-Transverse*, *Nucl. Phys. B* **197** (1982) 446 [InSPIRE].

[69] P. Nason, *A New method for combining NLO QCD with shower Monte Carlo algorithms*, *JHEP* **11** (2004) 040 [hep-ph/0409146] [InSPIRE].

[70] S. Frixione, P. Nason and C. Oleari, *Matching NLO QCD computations with Parton Shower simulations: the POWHEG method*, *JHEP* **11** (2007) 070 [arXiv:0709.2092] [InSPIRE].

[71] S. Alioli, P. Nason, C. Oleari and E. Re, *NLO vector-boson production matched with shower in POWHEG*, *JHEP* **07** (2008) 060 [arXiv:0805.4802] [InSPIRE].

[72] S. Alioli, P. Nason, C. Oleari and E. Re, *A general framework for implementing NLO calculations in shower Monte Carlo programs: the POWHEG BOX*, *JHEP* **06** (2010) 043 [arXiv:1002.2581] [InSPIRE].

[73] M. Bahr et al., *HERWIG++ Physics and Manual*, *Eur. Phys. J. C* **58** (2008) 639 [arXiv:0803.0883] [InSPIRE].

[74] J. Bellm et al., *HERWIG 7.0/HERWIG++ 3.0 release note*, *Eur. Phys. J. C* **76** (2016) 196 [arXiv:1512.01178] [InSPIRE].

[75] S. Alekhin, J. Blumlein and S. Moch, *The ABM parton distributions tuned to LHC data*, *Phys. Rev. D* **89** (2014) 054028 [arXiv:1310.3059] [InSPIRE].

[76] NNPDF collaboration, *Parton distributions from high-precision collider data*, *Eur. Phys. J. C* **77** (2017) 663 [arXiv:1706.00428] [InSPIRE].

[77] H.-L. Lai et al., *Parton Distributions for Event Generators*, *JHEP* **04** (2010) 035 [arXiv:0910.4183] [InSPIRE].

[78] P. Skands, S. Carrazza and J. Rojo, *Tuning PYTHIA 8.1: the Monash 2013 Tune*, *Eur. Phys. J. C* **74** (2014) 3024 [arXiv:1404.5630] [InSPIRE].

The LHCb collaboration

R. Aaij,[32] A.S.W. Abdelmotteleb,[56] C. Abellán Beteta,[50] F. Abudinén,[56] T. Ackernley,[60] B. Adeva,[46] M. Adinolfi,[54] H. Afsharnia,[9] C. Agapopoulou,[13] C.A. Aidala,[87] S. Aiola,[25] Z. Ajaltouni,[9] S. Akar,[65] J. Albrecht,[15] F. Alessio,[48] M. Alexander,[59] A. Alfonso Albero,[45] Z. Aliouche,[62] G. Alkhazov,[38] P. Alvarez Cartelle,[55] S. Amato,[2] J.L. Amey,[54] Y. Amhis,[11] L. An,[48] L. Anderlini,[22] M. Andersson,[50] A. Andreianov,[38] M. Andreotti,[21] F. Archilli,[17] A. Artamonov,[44] M. Artuso,[68] K. Arzymatov,[42] E. Aslanides,[10] M. Atzeni,[50] B. Audurier,[12] S. Bachmann,[17] M. Bachmayer,[49] J.J. Back,[56] P. Baladron Rodriguez,[46] V. Balagura,[12] W. Baldini,[21] J. Baptista de Souza Leite,[1] M. Barbetti,[22,h] R.J. Barlow,[62] S. Barsuk,[11] W. Barter,[61] M. Bartolini,[55] F. Baryshnikov,[83] J.M. Basels,[14] S. Bashir,[34] G. Bassi,[29] B. Batsukh,[68] A. Battig,[15] A. Bay,[49] A. Beck,[56] M. Becker,[15] F. Bedeschi,[29] I. Bediaga,[1] A. Beiter,[68] V. Belavin,[42] S. Belin,[27] V. Bellee,[50] K. Belous,[44] I. Belov,[40] I. Belyaev,[41] G. Bencivenni,[23] E. Ben-Haim,[13] A. Berezhnoy,[40] R. Bernet,[50] D. Berninghoff,[17] H.C. Bernstein,[68] C. Bertella,[62] A. Bertolin,[28] C. Betancourt,[50] F. Betti,[48] I. Bezshyiko,[50] S. Bhasin,[54] J. Bhom,[35] L. Bian,[73] M.S. Bieker,[15] N.V. Biesuz,[21] S. Bifani,[53] P. Billoir,[13] A. Biolchini,[32] M. Birch,[61] F.C.R. Bishop,[55] A. Bitadze,[62] A. Bizzeti,[22,l] M. Bjørn,[63] M.P. Blago,[48] T. Blake,[56] F. Blanc,[49] S. Blusk,[68] D. Bobulska,[59] J.A. Boelhauve,[15] O. Boente Garcia,[46] T. Boettcher,[65] A. Boldyrev,[82] A. Bondar,[43] N. Bondar,[38,48] S. Borghi,[62] M. Borisyak,[42] M. Borsato,[17] J.T. Borsuk,[35] S.A. Bouchiba,[49] T.J.V. Bowcock,[60,48] A. Boyer,[48] C. Bozzi,[21] M.J. Bradley,[61] S. Braun,[66] A. Brea Rodriguez,[46] J. Brodzicka,[35] A. Brossa Gonzalo,[56] D. Brundu,[27] A. Buonaura,[50] L. Buonincontri,[28] A.T. Burke,[62] C. Burr,[48] A. Bursche,[72] A. Butkevich,[39] J.S. Butter,[32] J. Buytaert,[48] W. Byczynski,[48] S. Cadeddu,[27] H. Cai,[73] R. Calabrese,[21,g] L. Calefice,[15,13] S. Cali,[23] R. Calladine,[53] M. Calvi,[26,k] M. Calvo Gomez,[85] P. Camargo Magalhaes,[54] P. Campana,[23] A.F. Campoverde Quezada,[6] S. Capelli,[26,k] L. Capriotti,[20,e] A. Carbone,[20,e] G. Carboni,[31,q] R. Cardinale,[24,i] A. Cardini,[27] I. Carli,[4] P. Carniti,[26,k] L. Carus,[14] K. Carvalho Akiba,[32] A. Casais Vidal,[46] R. Caspary,[17] G. Casse,[60] M. Cattaneo,[48] G. Cavallero,[48] S. Celani,[49] J. Cerasoli,[10] D. Cervenkov,[63] A.J. Chadwick,[60] M.G. Chapman,[54] M. Charles,[13] P. Charpentier,[48] G. Chatzikonstantinidis,[53] C.A. Chavez Barajas,[60] M. Chefdeville,[8] C. Chen,[3] S. Chen,[4] A. Chernov,[35] V. Chobanova,[46] S. Cholak,[49] M. Chrzaszcz,[35] A. Chubykin,[38] V. Chulikov,[38] P. Ciambrone,[23] M.F. Cicala,[56] X. Cid Vidal,[46] G. Ciezarek,[48] P.E.L. Clarke,[58] M. Clemencic,[48] H.V. Cliff,[55] J. Closier,[48] J.L. Cobbledick,[62] V. Coco,[48] J.A.B. Coelho,[11] J. Cogan,[10] E. Cogneras,[9] L. Cojocariu,[37] P. Collins,[48] T. Colombo,[48] L. Congedo,[19,d] A. Contu,[27] N. Cooke,[53] G. Coombs,[59] I. Corredoira,[46] G. Corti,[48] C.M. Costa Sobral,[56] B. Couturier,[48] D.C. Craik,[64] J. Crkovská,[67] M. Cruz Torres,[1] R. Currie,[58] C.L. Da Silva,[67] S. Dadabaev,[83] L. Dai,[71] E. Dall'Occo,[15] J. Dalseno,[46] C. D'Ambrosio,[48] A. Danilina,[41] P. d'Argent,[48] A. Dashkina,[83] J.E. Davies,[62] A. Davis,[62] O. De Aguiar Francisco,[62] K. De Bruyn,[79] S. De Capua,[62] M. De Cian,[49] E. De Lucia,[23] J.M. De Miranda,[1] L. De Paula,[2] M. De Serio,[19,d] D. De Simone,[50] P. De Simone,[23] F. De Vellis,[15] J.A. de Vries,[80] C.T. Dean,[67] F. Debernardis,[19,d] D. Decamp,[8] V. Dedu,[10] L. Del Buono,[13] B. Delaney,[55] H.-P. Dembinski,[15] A. Dendek,[34] V. Denysenko,[50] D. Derkach,[82] O. Deschamps,[9] F. Desse,[11] F. Dettori,[27,f] B. Dey,[77] A. Di Cicco,[23] P. Di Nezza,[23] S. Didenko,[83] L. Dieste Maronas,[46] H. Dijkstra,[48] V. Dobishuk,[52] C. Dong,[3] A.M. Donohoe,[18] F. Dordei,[27] A.C. dos Reis,[1] L. Douglas,[59] A. Dovbnya,[51] A.G. Downes,[8] M.W. Dudek,[35] L. Dufour,[48] V. Duk,[78] P. Durante,[48] J.M. Durham,[67] D. Dutta,[62] A. Dziurda,[35] A. Dzyuba,[38] S. Easo,[57] U. Egede,[69] V. Egorychev,[41] S. Eidelman,[43,v,†] S. Eisenhardt,[58] S. Ek-In,[49] L. Eklund,[86] S. Ely,[68] A. Ene,[37] E. Epple,[67] S. Escher,[14] J. Eschle,[50] S. Esen,[50] T. Evans,[48] L.N. Falcao,[1] Y. Fan,[6] B. Fang,[73] S. Farry,[60]

D. Fazzini,[26,k] M. Féo,[48] A. Fernandez Prieto,[46] A.D. Fernez,[66] F. Ferrari,[20,e]
L. Ferreira Lopes,[49] F. Ferreira Rodrigues,[2] S. Ferreres Sole,[32] M. Ferrillo,[50] M. Ferro-Luzzi,[48]
S. Filippov,[39] R.A. Fini,[19] M. Fiorini,[21,g] M. Firlej,[34] K.M. Fischer,[63] D.S. Fitzgerald,[87]
C. Fitzpatrick,[62] T. Fiutowski,[34] A. Fkiaras,[48] F. Fleuret,[12] M. Fontana,[13] F. Fontanelli,[24,i]
R. Forty,[48] D. Foulds-Holt,[55] V. Franco Lima,[60] M. Franco Sevilla,[66] M. Frank,[48]
E. Franzoso,[21] G. Frau,[17] C. Frei,[48] D.A. Friday,[59] J. Fu,[6] Q. Fuehring,[15] E. Gabriel,[32]
G. Galati,[19,d] A. Gallas Torreira,[46] D. Galli,[20,e] S. Gambetta,[58,48] Y. Gan,[3] M. Gandelman,[2]
P. Gandini,[25] Y. Gao,[5] M. Garau,[27] L.M. Garcia Martin,[56] P. Garcia Moreno,[45]
J. García Pardiñas,[26,k] B. Garcia Plana,[46] F.A. Garcia Rosales,[12] L. Garrido,[45] C. Gaspar,[48]
R.E. Geertsema,[32] D. Gerick,[17] L.L. Gerken,[15] E. Gersabeck,[62] M. Gersabeck,[62] T. Gershon,[56]
D. Gerstel,[10] L. Giambastiani,[28] V. Gibson,[55] H.K. Giemza,[36] A.L. Gilman,[63]
M. Giovannetti,[23,q] A. Gioventù,[46] P. Gironella Gironell,[45] C. Giugliano,[21,g] K. Gizdov,[58]
E.L. Gkougkousis,[48] V.V. Gligorov,[13] C. Göbel,[70] E. Golobardes,[85] D. Golubkov,[41]
A. Golutvin,[61,83] A. Gomes,[1,a] S. Gomez Fernandez,[45] F. Goncalves Abrantes,[63] M. Goncerz,[35]
G. Gong,[3] P. Gorbounov,[41] I.V. Gorelov,[40] C. Gotti,[26] E. Govorkova,[48] J.P. Grabowski,[17]
T. Grammatico,[13] L.A. Granado Cardoso,[48] E. Graugés,[45] E. Graverini,[49] G. Graziani,[22]
A. Grecu,[37] L.M. Greeven,[32] N.A. Grieser,[4] L. Grillo,[62] S. Gromov,[83] B.R. Gruberg Cazon,[63]
C. Gu,[3] M. Guarise,[21] M. Guittiere,[11] P.A. Günther,[17] E. Gushchin,[39] A. Guth,[14] Y. Guz,[44]
T. Gys,[48] T. Hadavizadeh,[69] G. Haefeli,[49] C. Haen,[48] J. Haimberger,[48] T. Halewood-leagas,[60]
P.M. Hamilton,[66] J.P. Hammerich,[60] Q. Han,[7] X. Han,[17] T.H. Hancock,[63] E.B. Hansen,[62]
S. Hansmann-Menzemer,[17] N. Harnew,[63] T. Harrison,[60] C. Hasse,[48] M. Hatch,[48] J. He,[6,b]
M. Hecker,[61] K. Heijhoff,[32] K. Heinicke,[15] R.D.L. Henderson,[69,56] A.M. Hennequin,[48]
K. Hennessy,[60] L. Henry,[48] J. Heuel,[14] A. Hicheur,[2] D. Hill,[49] M. Hilton,[62] S.E. Hollitt,[15]
R. Hou,[7] Y. Hou,[8] J. Hu,[17] J. Hu,[72] W. Hu,[7] X. Hu,[3] W. Huang,[6] X. Huang,[73]
W. Hulsbergen,[32] R.J. Hunter,[56] M. Hushchyn,[82] D. Hutchcroft,[60] D. Hynds,[32] P. Ibis,[15]
M. Idzik,[34] D. Ilin,[38] P. Ilten,[65] A. Inglessi,[38] A. Ishteev,[83] K. Ivshin,[38] R. Jacobsson,[48]
H. Jage,[14] S. Jakobsen,[48] E. Jans,[32] B.K. Jashal,[47] A. Jawahery,[66] V. Jevtic,[15] X. Jiang,[4]
M. John,[63] D. Johnson,[64] C.R. Jones,[55] T.P. Jones,[56] B. Jost,[48] N. Jurik,[48]
S.H. Kalavan Kadavath,[34] S. Kandybei,[51] Y. Kang,[3] M. Karacson,[48] M. Karpov,[82]
J.W. Kautz,[65] F. Keizer,[48] D.M. Keller,[68] M. Kenzie,[56] T. Ketel,[33] B. Khanji,[15]
A. Kharisova,[84] S. Kholodenko,[44] T. Kirn,[14] V.S. Kirsebom,[49] O. Kitouni,[64] S. Klaver,[32]
N. Kleijne,[29] K. Klimaszewski,[36] M.R. Kmiec,[36] S. Koliiev,[52] A. Kondybayeva,[83]
A. Konoplyannikov,[41] P. Kopciewicz,[34] R. Kopecna,[17] P. Koppenburg,[32] M. Korolev,[40]
I. Kostiuk,[32,52] O. Kot,[52] S. Kotriakhova,[21,38] P. Kravchenko,[38] L. Kravchuk,[39]
R.D. Krawczyk,[48] M. Kreps,[56] F. Kress,[61] S. Kretzschmar,[14] P. Krokovny,[43,v] W. Krupa,[34]
W. Krzemien,[36] J. Kubat,[17] M. Kucharczyk,[35] V. Kudryavtsev,[43,v] H.S. Kuindersma,[32,33]
G.J. Kunde,[67] T. Kvaratskheliya,[41] D. Lacarrere,[48] G. Lafferty,[62] A. Lai,[27] A. Lampis,[27]
D. Lancierini,[50] J.J. Lane,[62] R. Lane,[54] G. Lanfranchi,[23] C. Langenbruch,[14] J. Langer,[15]
O. Lantwin,[83] T. Latham,[56] F. Lazzari,[29,r] R. Le Gac,[10] S.H. Lee,[87] R. Lefèvre,[9] A. Leflat,[40]
S. Legotin,[83] O. Leroy,[10] T. Lesiak,[35] B. Leverington,[17] H. Li,[72] P. Li,[17] S. Li,[7] Y. Li,[4]
Y. Li,[4] Z. Li,[68] X. Liang,[68] T. Lin,[61] R. Lindner,[48] V. Lisovskyi,[15] R. Litvinov,[27] G. Liu,[72]
H. Liu,[6] Q. Liu,[6] S. Liu,[4] A. Lobo Salvia,[45] A. Loi,[27] J. Lomba Castro,[46] I. Longstaff,[59]
J.H. Lopes,[2] S. López Soliño,[46] G.H. Lovell,[55] Y. Lu,[4] C. Lucarelli,[22,h] D. Lucchesi,[28,m]
S. Luchuk,[39] M. Lucio Martinez,[32] V. Lukashenko,[32,52] Y. Luo,[3] A. Lupato,[62] E. Luppi,[21,g]
O. Lupton,[56] A. Lusiani,[29,n] X. Lyu,[6] L. Ma,[4] R. Ma,[6] S. Maccolini,[20,e] F. Machefert,[11]
F. Maciuc,[37] V. Macko,[49] P. Mackowiak,[15] S. Maddrell-Mander,[54] O. Madejczyk,[34]
L.R. Madhan Mohan,[54] O. Maev,[38] A. Maevskiy,[82] M.W. Majewski,[34] J.J. Malczewski,[35]
S. Malde,[63] B. Malecki,[48] A. Malinin,[81] T. Maltsev,[43,v] H. Malygina,[17] G. Manca,[27,f]
G. Mancinelli,[10] D. Manuzzi,[20,e] D. Marangotto,[25,j] J. Maratas,[9,t] J.F. Marchand,[8]

U. Marconi,[20] S. Mariani,[22,h] C. Marin Benito,[48] M. Marinangeli,[49] J. Marks,[17]
A.M. Marshall,[54] P.J. Marshall,[60] G. Martelli,[78] G. Martellotti,[30] L. Martinazzoli,[48,k]
M. Martinelli,[26,k] D. Martinez Santos,[46] F. Martinez Vidal,[47] A. Massafferri,[1] M. Materok,[14]
R. Matev,[48] A. Mathad,[50] V. Matiunin,[41] C. Matteuzzi,[26] K.R. Mattioli,[87] A. Mauri,[32]
E. Maurice,[12] J. Mauricio,[45] M. Mazurek,[48] M. McCann,[61] L. Mcconnell,[18] T.H. Mcgrath,[62]
N.T. Mchugh,[59] A. McNab,[62] R. McNulty,[18] J.V. Mead,[60] B. Meadows,[65] G. Meier,[15]
D. Melnychuk,[36] S. Meloni,[26,k] M. Merk,[32,80] A. Merli,[25,j] L. Meyer Garcia,[2]
M. Mikhasenko,[75,c] D.A. Milanes,[74] E. Millard,[56] M. Milovanovic,[48] M.-N. Minard,[8]
A. Minotti,[26,k] L. Minzoni,[21,g] S.E. Mitchell,[58] B. Mitreska,[62] D.S. Mitzel,[15] A. Mödden,[15]
R.A. Mohammed,[63] R.D. Moise,[61] S. Mokhnenko,[82] T. Mombächer,[46] I.A. Monroy,[74]
S. Monteil,[9] M. Morandin,[28] G. Morello,[23] M.J. Morello,[29,n] J. Moron,[34] A.B. Morris,[75]
A.G. Morris,[56] R. Mountain,[68] H. Mu,[3] F. Muheim,[58,48] M. Mulder,[79] D. Müller,[48]
K. Müller,[50] C.H. Murphy,[63] D. Murray,[62] R. Murta,[61] P. Muzzetto,[27] P. Naik,[54]
T. Nakada,[49] R. Nandakumar,[57] T. Nanut,[48] I. Nasteva,[2] M. Needham,[58] N. Neri,[25,j]
S. Neubert,[75] N. Neufeld,[48] R. Newcombe,[61] E.M. Niel,[11] S. Nieswand,[14] N. Nikitin,[40]
N.S. Nolte,[64] C. Normand,[8] C. Nunez,[87] A. Oblakowska-Mucha,[34] V. Obraztsov,[44] T. Oeser,[14]
D.P. O'Hanlon,[54] S. Okamura,[21] R. Oldeman,[27,f] F. Oliva,[58] M.E. Olivares,[68]
C.J.G. Onderwater,[79] R.H. O'Neil,[58] J.M. Otalora Goicochea,[2] T. Ovsiannikova,[41] P. Owen,[50]
A. Oyanguren,[47] K.O. Padeken,[75] B. Pagare,[56] P.R. Pais,[48] T. Pajero,[63] A. Palano,[19]
M. Palutan,[23] Y. Pan,[62] G. Panshin,[84] A. Papanestis,[57] M. Pappagallo,[19,d]
L.L. Pappalardo,[21,g] C. Pappenheimer,[65] W. Parker,[66] C. Parkes,[62] B. Passalacqua,[21]
G. Passaleva,[22] A. Pastore,[19] M. Patel,[61] C. Patrignani,[20,e] C.J. Pawley,[80] A. Pearce,[48,57]
A. Pellegrino,[32] M. Pepe Altarelli,[48] S. Perazzini,[20] D. Pereima,[41] A. Pereiro Castro,[46]
P. Perret,[9] M. Petric,[59,48] K. Petridis,[54] A. Petrolini,[24,i] A. Petrov,[81] S. Petrucci,[58]
M. Petruzzo,[25] T.T.H. Pham,[68] A. Philippov,[42] R. Piandani,[6] L. Pica,[29,n] M. Piccini,[78]
B. Pietrzyk,[8] G. Pietrzyk,[49] M. Pili,[63] D. Pinci,[30] F. Pisani,[48] M. Pizzichemi,[26,48,k]
P.K. Resmi,[10] V. Placinta,[37] J. Plews,[53] M. Plo Casasus,[46] F. Polci,[13] M. Poli Lener,[23]
M. Poliakova,[68] A. Poluektov,[10] N. Polukhina,[83,u] I. Polyakov,[68] E. Polycarpo,[2] S. Ponce,[48]
D. Popov,[6,48] S. Popov,[42] S. Poslavskii,[44] K. Prasanth,[35] L. Promberger,[48] C. Prouve,[46]
V. Pugatch,[52] V. Puill,[11] G. Punzi,[29,o] H. Qi,[3] W. Qian,[6] N. Qin,[3] Y. Qiu,[7] R. Quagliani,[49]
N.V. Raab,[18] R.I. Rabadan Trejo,[6] B. Rachwal,[34] J.H. Rademacker,[54] M. Rama,[29]
M. Ramos Pernas,[56] M.S. Rangel,[2] F. Ratnikov,[42,82] G. Raven,[33] M. Reboud,[8] F. Redi,[49]
F. Reiss,[62] C. Remon Alepuz,[47] Z. Ren,[3] V. Renaudin,[63] R. Ribatti,[29] A.M. Ricci,[27]
S. Ricciardi,[57] K. Rinnert,[60] P. Robbe,[11] G. Robertson,[58] A.B. Rodrigues,[49] E. Rodrigues,[60]
J.A. Rodriguez Lopez,[74] E.R.R. Rodriguez Rodriguez,[46] A. Rollings,[63] P. Roloff,[48]
V. Romanovskiy,[44] M. Romero Lamas,[46] A. Romero Vidal,[46] J.D. Roth,[87] M. Rotondo,[23]
M.S. Rudolph,[68] T. Ruf,[48] R.A. Ruiz Fernandez,[46] J. Ruiz Vidal,[47] A. Ryzhikov,[82] J. Ryzka,[34]
J.J. Saborido Silva,[46] N. Sagidova,[38] N. Sahoo,[56] B. Saitta,[27,f] M. Salomoni,[48]
C. Sanchez Gras,[32] R. Santacesaria,[30] C. Santamarina Rios,[46] M. Santimaria,[23]
E. Santovetti,[31,q] D. Saranin,[83] G. Sarpis,[14] M. Sarpis,[75] A. Sarti,[30] C. Satriano,[30,p]
A. Satta,[31] M. Saur,[15] D. Savrina,[41,40] H. Sazak,[9] L.G. Scantlebury Smead,[63] A. Scarabotto,[13]
S. Schael,[14] S. Scherl,[60] M. Schiller,[59] H. Schindler,[48] M. Schmelling,[16] B. Schmidt,[48]
S. Schmitt,[14] O. Schneider,[49] A. Schopper,[48] M. Schubiger,[32] S. Schulte,[49] M.H. Schune,[11]
R. Schwemmer,[48] B. Sciascia,[23,48] S. Sellam,[46] A. Semennikov,[41] M. Senghi Soares,[33]
A. Sergi,[24,i] N. Serra,[50] L. Sestini,[28] A. Seuthe,[15] Y. Shang,[5] D.M. Shangase,[87] M. Shapkin,[44]
I. Shchemerov,[83] L. Shchutska,[49] T. Shears,[60] L. Shekhtman,[43,v] Z. Shen,[5] S. Sheng,[4]
V. Shevchenko,[81] E.B. Shields,[26,k] Y. Shimizu,[11] E. Shmanin,[83] J.D. Shupperd,[68]
B.G. Siddi,[21] R. Silva Coutinho,[50] G. Simi,[28] S. Simone,[19,d] N. Skidmore,[62] T. Skwarnicki,[68]
M.W. Slater,[53] I. Slazyk,[21,g] J.C. Smallwood,[63] J.G. Smeaton,[55] A. Smetkina,[41] E. Smith,[50]

M. Smith,[61] A. Snoch,[32] L. Soares Lavra,[9] M.D. Sokoloff,[65] F.J.P. Soler,[59] A. Solovev,[38]
I. Solovyev,[38] F.L. Souza De Almeida,[2] B. Souza De Paula,[2] B. Spaan,[15]
E. Spadaro Norella,[25,j] P. Spradlin,[59] F. Stagni,[48] M. Stahl,[65] S. Stahl,[48] S. Stanislaus,[63]
O. Steinkamp,[50,83] O. Stenyakin,[44] H. Stevens,[15] S. Stone,[68,48] D. Strekalina,[83] F. Suljik,[63]
J. Sun,[27] L. Sun,[73] Y. Sun,[66] P. Svihra,[62] P.N. Swallow,[53] K. Swientek,[34] A. Szabelski,[36]
T. Szumlak,[34] M. Szymanski,[48] S. Taneja,[62] A.R. Tanner,[54] M.D. Tat,[63] A. Terentev,[83]
F. Teubert,[48] E. Thomas,[48] D.J.D. Thompson,[53] K.A. Thomson,[60] H. Tilquin,[61]
V. Tisserand,[9] S. T'Jampens,[8] M. Tobin,[4] L. Tomassetti,[21,g] X. Tong,[5] D. Torres Machado,[1]
D.Y. Tou,[13] E. Trifonova,[83] S.M. Trilov,[54] C. Trippl,[49] G. Tuci,[6] A. Tully,[49] N. Tuning,[32,48]
A. Ukleja,[36,48] D.J. Unverzagt,[17] E. Ursov,[83] A. Usachov,[32] A. Ustyuzhanin,[42,82] U. Uwer,[17]
A. Vagner,[84] V. Vagnoni,[20] A. Valassi,[48] G. Valenti,[20] N. Valls Canudas,[85]
M. van Beuzekom,[32] M. Van Dijk,[49] H. Van Hecke,[67] E. van Herwijnen,[83] M. van Veghel,[79]
R. Vazquez Gomez,[45] P. Vazquez Regueiro,[46] C. Vázquez Sierra,[48] S. Vecchi,[21] J.J. Velthuis,[54]
M. Veltri,[22,s] A. Venkateswaran,[68] M. Veronesi,[32] M. Vesterinen,[56] D. Vieira,[65]
M. Vieites Diaz,[49] H. Viemann,[76] X. Vilasis-Cardona,[85] E. Vilella Figueras,[60] A. Villa,[20]
P. Vincent,[13] F.C. Volle,[11] D. Vom Bruch,[10] A. Vorobyev,[38] V. Vorobyev,[43,v] N. Voropaev,[38]
K. Vos,[80] R. Waldi,[17] J. Walsh,[29] C. Wang,[17] J. Wang,[5] J. Wang,[4] J. Wang,[3] J. Wang,[73]
M. Wang,[3] R. Wang,[54] Y. Wang,[7] Z. Wang,[50] Z. Wang,[3] Z. Wang,[6] J.A. Ward,[56,69]
N.K. Watson,[53] S.G. Weber,[13] D. Websdale,[61] C. Weisser,[64] B.D.C. Westhenry,[54]
D.J. White,[62] M. Whitehead,[54] A.R. Wiederhold,[56] D. Wiedner,[15] G. Wilkinson,[63]
M. Wilkinson,[68] I. Williams,[55] M. Williams,[64] M.R.J. Williams,[58] F.F. Wilson,[57]
W. Wislicki,[36] M. Witek,[35] L. Witola,[17] G. Wormser,[11] S.A. Wotton,[55] H. Wu,[68] K. Wyllie,[48]
Z. Xiang,[6] D. Xiao,[7] Y. Xie,[7] A. Xu,[5] J. Xu,[6] L. Xu,[3] M. Xu,[56] Q. Xu,[6] Z. Xu,[9] Z. Xu,[6]
D. Yang,[3] S. Yang,[6] Y. Yang,[6] Z. Yang,[5] Z. Yang,[66] Y. Yao,[68] L.E. Yeomans,[60] H. Yin,[7]
J. Yu,[71] X. Yuan,[68] O. Yushchenko,[44] E. Zaffaroni,[49] M. Zavertyaev,[16,u] M. Zdybal,[35]
O. Zenaiev,[48] M. Zeng,[3] D. Zhang,[7] L. Zhang,[3] S. Zhang,[71] S. Zhang,[5] Y. Zhang,[5]
Y. Zhang,[63] A. Zharkova,[83] A. Zhelezov,[17] Y. Zheng,[6] T. Zhou,[5] X. Zhou,[6] Y. Zhou,[6]
V. Zhovkovska,[11] X. Zhu,[3] X. Zhu,[7] Z. Zhu,[6] V. Zhukov,[14,40] J.B. Zonneveld,[58] Q. Zou,[4]
S. Zucchelli,[20,e] D. Zuliani,[28] G. Zunica[62]

1. *Centro Brasileiro de Pesquisas Físicas (CBPF), Rio de Janeiro, Brazil*
2. *Universidade Federal do Rio de Janeiro (UFRJ), Rio de Janeiro, Brazil*
3. *Center for High Energy Physics, Tsinghua University, Beijing, China*
4. *Institute Of High Energy Physics (IHEP), Beijing, China*
5. *School of Physics State Key Laboratory of Nuclear Physics and Technology, Peking University, Beijing, China*
6. *University of Chinese Academy of Sciences, Beijing, China*
7. *Institute of Particle Physics, Central China Normal University, Wuhan, Hubei, China*
8. *Univ. Savoie Mont Blanc, CNRS, IN2P3-LAPP, Annecy, France*
9. *Université Clermont Auvergne, CNRS/IN2P3, LPC, Clermont-Ferrand, France*
10. *Aix Marseille Univ, CNRS/IN2P3, CPPM, Marseille, France*
11. *Université Paris-Saclay, CNRS/IN2P3, IJCLab, Orsay, France*
12. *Laboratoire Leprince-Ringuet, CNRS/IN2P3, Ecole Polytechnique, Institut Polytechnique de Paris, Palaiseau, France*
13. *LPNHE, Sorbonne Université, Paris Diderot Sorbonne Paris Cité, CNRS/IN2P3, Paris, France*
14. *I. Physikalisches Institut, RWTH Aachen University, Aachen, Germany*
15. *Fakultät Physik, Technische Universität Dortmund, Dortmund, Germany*
16. *Max-Planck-Institut für Kernphysik (MPIK), Heidelberg, Germany*
17. *Physikalisches Institut, Ruprecht-Karls-Universität Heidelberg, Heidelberg, Germany*
18. *School of Physics, University College Dublin, Dublin, Ireland*

19 *INFN Sezione di Bari, Bari, Italy*
20 *INFN Sezione di Bologna, Bologna, Italy*
21 *INFN Sezione di Ferrara, Ferrara, Italy*
22 *INFN Sezione di Firenze, Firenze, Italy*
23 *INFN Laboratori Nazionali di Frascati, Frascati, Italy*
24 *INFN Sezione di Genova, Genova, Italy*
25 *INFN Sezione di Milano, Milano, Italy*
26 *INFN Sezione di Milano-Bicocca, Milano, Italy*
27 *INFN Sezione di Cagliari, Monserrato, Italy*
28 *Università degli Studi di Padova, Università e INFN, Padova, Padova, Italy*
29 *INFN Sezione di Pisa, Pisa, Italy*
30 *INFN Sezione di Roma La Sapienza, Roma, Italy*
31 *INFN Sezione di Roma Tor Vergata, Roma, Italy*
32 *Nikhef National Institute for Subatomic Physics, Amsterdam, The Netherlands*
33 *Nikhef National Institute for Subatomic Physics and VU University Amsterdam, Amsterdam, The Netherlands*
34 *AGH — University of Science and Technology, Faculty of Physics and Applied Computer Science, Kraków, Poland*
35 *Henryk Niewodniczanski Institute of Nuclear Physics Polish Academy of Sciences, Kraków, Poland*
36 *National Center for Nuclear Research (NCBJ), Warsaw, Poland*
37 *Horia Hulubei National Institute of Physics and Nuclear Engineering, Bucharest-Magurele, Romania*
38 *Petersburg Nuclear Physics Institute NRC Kurchatov Institute (PNPI NRC KI), Gatchina, Russia*
39 *Institute for Nuclear Research of the Russian Academy of Sciences (INR RAS), Moscow, Russia*
40 *Institute of Nuclear Physics, Moscow State University (SINP MSU), Moscow, Russia*
41 *Institute of Theoretical and Experimental Physics NRC Kurchatov Institute (ITEP NRC KI), Moscow, Russia*
42 *Yandex School of Data Analysis, Moscow, Russia*
43 *Budker Institute of Nuclear Physics (SB RAS), Novosibirsk, Russia*
44 *Institute for High Energy Physics NRC Kurchatov Institute (IHEP NRC KI), Protvino, Russia*
45 *ICCUB, Universitat de Barcelona, Barcelona, Spain*
46 *Instituto Galego de Física de Altas Enerxías (IGFAE), Universidade de Santiago de Compostela, Santiago de Compostela, Spain*
47 *Instituto de Fisica Corpuscular, Centro Mixto Universidad de Valencia — CSIC, Valencia, Spain*
48 *European Organization for Nuclear Research (CERN), Geneva, Switzerland*
49 *Institute of Physics, Ecole Polytechnique Fédérale de Lausanne (EPFL), Lausanne, Switzerland*
50 *Physik-Institut, Universität Zürich, Zürich, Switzerland*
51 *NSC Kharkiv Institute of Physics and Technology (NSC KIPT), Kharkiv, Ukraine*
52 *Institute for Nuclear Research of the National Academy of Sciences (KINR), Kyiv, Ukraine*
53 *University of Birmingham, Birmingham, U.K.*
54 *H.H. Wills Physics Laboratory, University of Bristol, Bristol, U.K.*
55 *Cavendish Laboratory, University of Cambridge, Cambridge, U.K.*
56 *Department of Physics, University of Warwick, Coventry, U.K.*
57 *STFC Rutherford Appleton Laboratory, Didcot, U.K.*
58 *School of Physics and Astronomy, University of Edinburgh, Edinburgh, U.K.*
59 *School of Physics and Astronomy, University of Glasgow, Glasgow, U.K.*
60 *Oliver Lodge Laboratory, University of Liverpool, Liverpool, U.K.*
61 *Imperial College London, London, U.K.*
62 *Department of Physics and Astronomy, University of Manchester, Manchester, U.K.*
63 *Department of Physics, University of Oxford, Oxford, U.K.*
64 *Massachusetts Institute of Technology, Cambridge, MA, U.S.A.*
65 *University of Cincinnati, Cincinnati, OH, U.S.A.*
66 *University of Maryland, College Park, MD, U.S.A.*

[67] *Los Alamos National Laboratory (LANL), Los Alamos, NM, U.S.A.*

[68] *Syracuse University, Syracuse, NY, U.S.A.*

[69] *School of Physics and Astronomy, Monash University, Melbourne, Australia, associated to [56]*

[70] *Pontifícia Universidade Católica do Rio de Janeiro (PUC-Rio), Rio de Janeiro, Brazil, associated to [2]*

[71] *Physics and Micro Electronic College, Hunan University, Changsha City, China, associated to [7]*

[72] *Guangdong Provincial Key Laboratory of Nuclear Science, Guangdong-Hong Kong Joint Laboratory of Quantum Matter, Institute of Quantum Matter, South China Normal University, Guangzhou, China, associated to [3]*

[73] *School of Physics and Technology, Wuhan University, Wuhan, China, associated to [3]*

[74] *Departamento de Fisica, Universidad Nacional de Colombia, Bogota, Colombia, associated to [13]*

[75] *Universität Bonn — Helmholtz-Institut für Strahlen und Kernphysik, Bonn, Germany, associated to [17]*

[76] *Institut für Physik, Universität Rostock, Rostock, Germany, associated to [17]*

[77] *Eotvos Lorand University, Budapest, Hungary, associated to [48]*

[78] *INFN Sezione di Perugia, Perugia, Italy, associated to [21]*

[79] *Van Swinderen Institute, University of Groningen, Groningen, The Netherlands, associated to [32]*

[80] *Universiteit Maastricht, Maastricht, The Netherlands, associated to [32]*

[81] *National Research Centre Kurchatov Institute, Moscow, Russia, associated to [41]*

[82] *National Research University Higher School of Economics, Moscow, Russia, associated to [42]*

[83] *National University of Science and Technology "MISIS", Moscow, Russia, associated to [41]*

[84] *National Research Tomsk Polytechnic University, Tomsk, Russia, associated to [41]*

[85] *DS4DS, La Salle, Universitat Ramon Llull, Barcelona, Spain, associated to [45]*

[86] *Department of Physics and Astronomy, Uppsala University, Uppsala, Sweden, associated to [59]*

[87] *University of Michigan, Ann Arbor, U.S.A., associated to [68]*

[a] *Universidade Federal do Triângulo Mineiro (UFTM), Uberaba-MG, Brazil*

[b] *Hangzhou Institute for Advanced Study, UCAS, Hangzhou, China*

[c] *Excellence Cluster ORIGINS, Munich, Germany*

[d] *Università di Bari, Bari, Italy*

[e] *Università di Bologna, Bologna, Italy*

[f] *Università di Cagliari, Cagliari, Italy*

[g] *Università di Ferrara, Ferrara, Italy*

[h] *Università di Firenze, Firenze, Italy*

[i] *Università di Genova, Genova, Italy*

[j] *Università degli Studi di Milano, Milano, Italy*

[k] *Università di Milano Bicocca, Milano, Italy*

[l] *Università di Modena e Reggio Emilia, Modena, Italy*

[m] *Università di Padova, Padova, Italy*

[n] *Scuola Normale Superiore, Pisa, Italy*

[o] *Università di Pisa, Pisa, Italy*

[p] *Università della Basilicata, Potenza, Italy*

[q] *Università di Roma Tor Vergata, Roma, Italy*

[r] *Università di Siena, Siena, Italy*

[s] *Università di Urbino, Urbino, Italy*

[t] *MSU — Iligan Institute of Technology (MSU-IIT), Iligan, Philippines*

[u] *P.N. Lebedev Physical Institute, Russian Academy of Science (LPI RAS), Moscow, Russia*

[v] *Novosibirsk State University, Novosibirsk, Russia*

[†] *Deceased*